

# Performance Analysis of Distributed Intelligent Reflective Surfaces for Wireless Communications

Diluka Loku Galappaththige, *Student Member, IEEE*, Dhanushka Kudathanthirige, *Student Member, IEEE*, and Gayan Amarasuriya Aruma Baduge, *Senior Member, IEEE*

## Abstract

In this paper, a comprehensive performance analysis of a distributed intelligent reflective surfaces (IRS)-aided communication system is presented. First, the optimal signal-to-noise ratio (SNR), which is attainable through the direct and reflected channels, is quantified by controlling the phase-shifts of the distributed IRS. Next, this optimal SNR is statistically characterized by deriving tight approximations to the exact probability density function (PDF) and cumulative distribution function (CDF) for Nakagami- $m$  fading. The accuracy/tightness of this statistical characterization is investigated by deriving the Kullback-Leibler divergence. Our PDF/CDF analysis is used to derive tight approximations/bounds for the outage probability, achievable rate, and average symbol error rate (SER) in closed-form. To obtain useful insights, the asymptotic outage probability and average SER are derived for the high SNR regime. Thereby, the achievable diversity order and array gains are quantified. Our asymptotic performance analysis reveals that the diversity order can be boosted by using distributed passive IRS without generating additional electromagnetic (EM) waves via active radio frequency chains. Our asymptotic rate analysis shows that the lower and upper rate bounds converge to an asymptotic limit in large reflective element regime in which the transmit power can be scaled inversely proportional to the square of the number of reflective elements. Our analysis is validated via Monte-Carlo simulations. We present a rigorous set of numerical results to investigate the performance gains of the proposed system model. Our analytical and numerical results reveal that the performance of single-input single-output wireless systems can be boosted by recycling the EM waves generated by a transmitter through distributed passive IRS reflections to enable constructive signal combining at a receiver.

The authors are with the Department of Electrical and Computer Engineering, Southern Illinois University, Carbondale, IL, USA, Email: {diluka.lg,dhanushka.kudathanthirige,gayan.baduge}@siu.edu. This work in part has been submitted to IEEE Global Communication Conference (Globecom), Dec., 2020 [1].

## I. INTRODUCTION

Recently, a novel concept of coating physical objects such as building wall and windows within a wireless propagation medium with intelligent reflective surfaces (IRS), which can interact with electromagnetic (EM) waves, has emerged [1]–[3]. By invoking the recent research developments of meta-surfaces [4], the feasibility of synthesizing the IRS has been explored [2]. An IRS consists of a large number of passive reflective elements, which can introduce controllable phase-shifts to incident EM waves. These phase-shifts can be intelligently controlled to enable a constructive addition of EM waves at a desired destination and thereby boosting the signal-to-noise ratio (SNR) of the end-to-end communication. Moreover, the IRS enables recycling of EM waves without generating additional signals via radio-frequency (RF) chains/amplifiers and thus enhancing the energy efficiency. The current state-of-the-art wireless systems, including conventional communication systems such as massive multiple-input multiple-output (MIMO), millimeter wave (mmWave) communication, and ultra-dense deployments of small cells consume a high amount of energy and a considerable hardware implementation cost [5]. Moreover, the emerging mmWave communications may suffer from high path-losses, penetration losses, and signal blockages. To this end, IRS-aided communication systems can potentially address the need of more greener, cost effective, and sustainable wireless connectivity by enabling control over the propagation environment by recycling EM signals. Furthermore, the recent developments in physics of meta-surfaces [4] may contribute to cost effective implementation of IRS-aided wireless systems. Thus, by intelligently controlling the phase-shifts introduced by the reflective elements, the IRS-assisted system can potentially overcome unfavorable propagation conditions, increase the coverage area while retaining a higher energy efficiency due to the passive reflective elements. Moreover, additional information can be embedded onto reflective coefficients, and computations can be performed at the IRS to enable a smart propagation environment [6]. Specifically, the joint encoding of information at the transmitter and IRS elements can be used to break the barriers of channel capacity [6]. Thus, the concept of IRS has a great potential of unveiling a paradigm-shift on how a controllable/smart wireless propagation can be exploited by wireless designers to reach the ultimate performance limits.

### A. *Related prior research*

In [2], the core architectural aspects of IRS for wireless communications are explored. In [4], prototypes of meta-surfaces and meta-tiles that can be used to coat objects embedded

within a smart wireless propagation environment are already developed. In [7], the ray-tracing techniques are used to develop novel propagation/path-loss models for IRS-assisted wireless communications. In [8], the path-loss models for IRS channels are designed based on the EM properties, and, these models are categorized into far-field, near-field beamforming, and near-field broadcasting. In [9], [10], the joint optimization of precoders at the base-station (BS) and phase-shifts at the IRS is investigated, and the proposed solutions are based on the semidefinite relaxation (SDR) and alternating optimization techniques. Reference [11] presents two computationally efficient algorithms to maximize the energy efficiency for the transmit power allocation based on alternating maximization adopting gradient descent method and sequential fractional programming approach. In [12], the fundamental performance metrics of IRS-assisted communication systems operating over Rayleigh fading are derived. Reference [13] explores the feasibility of exploiting statistical channel state information (CSI) to optimize phase-shift designs at the IRS to maximize the achievable spectral efficiency. In [14], the novel IRS-aided techniques are explored to boost the physical layer security aspects of wireless communications. In [15], the potential of the large intelligent surface (LIS)-assisted communication system in boosting the performance is investigated. In [16], the beamforming designs are investigated with a practical phase-shift at the IRS. In [17], the capacity regions of the IRS-aided two user multiple-access channel are characterized. Thereby, the algorithms to find the inner and outer bounds of the capacity region are proposed for a centralized IRS deployment. In [18], the impact of practically-viable/limited IRS control channels is investigated, and a passive beamformer design, which can achieve the asymptotic optimal received SNR under discrete reflection phase-shifts, is presented. Furthermore in [18], a resource allocation algorithm to maximize the asymptotic sum rate under the passive beamforming is proposed. In [19], the asymptotically achievable uplink sum rate of an IRS-aided system is analyzed deriving the rate distributions for Rician fading channels. Reference [20] investigates an IRS-assisted wireless system operating in Rician fading channels by adopting maximal ratio transmission (MRT) at the BS. In [21], a performance comparison between the spherical and two-dimensional (2D) LIS deployments is presented, and it is shown that former can provide wider coverage while having simpler positioning and flexible implementation over the 2D counterpart. In [22], an analytical framework for random rotation based IRS-assisted systems is presented, and four low-complexity schemes via selection-based and coding-based approaches are proposed. In [23], the joint optimization of active transmit and passive reflect beamforming is investigated to maximize the secrecy rate for an IRS-assisted

secure communication system. In [24], the impact of artificial noise on IRS-assisted secure communication is investigated.

This paper goes well beyond our related conference paper submission [1] by presenting the average symbol error rate (SER), asymptotic outage/SER analysis in high SNR regime, Kullback-Leibler (KL) divergence, diversity order, array/coding gain, achievable rate limits in large reflective element regime, and transmit power scaling laws for the distributed IRS-aided communication systems.

### *B. Motivation and our contribution*

The main contribution of this work is to derive performance metrics for the distributed IRS deployments over Nakagami- $m$  fading in closed-form. A common attribute of the above related prior research [7]–[15], [17]–[22] is that their system models consist of a single IRS. However, the concept of IRS was originally envisioned to coat physical objects distributed within a wireless propagation channel. To this end, the fundamental performance metrics of a distributed IRS-aided communication set-up have not yet been explored. To fill this important gap in IRS literature, in this paper, we present a statistical characterization of the end-to-end optimal SNR and the corresponding performance metrics of a distributed IRS-aided system operating over Nakagami- $m$  fading. Specifically, the optimal SNR is tightly approximated by using a mathematically tractable counterpart via the central limit theorem (CLT) because the optimal counterpart does not seem to be amenable to closed-form characterization of the performance metrics. Then, the exact probability density function (PDF) and cumulative distribution function (CDF) of this optimal SNR approximation are derived. We analytically validate the tightness of our PDF/CDF approximations via the KL divergence. By using our PDF/CDF analysis, the outage probability, the average SER, and achievable rate bounds/approximations are derived in closed-form. In order to obtain further insights, we report to an asymptotic analysis of the outage probability and average SER in the high SNR regime. Thereby, the achievable diversity order and array/coding gain are quantified. Our asymptotic analysis reveals that the achievable diversity order can be linearly increased with the product of the number of distributed IRSs and the number of elements in each IRS. This diversity order is achieved via passive reflections at the distributed IRS deployment via recycling existing EM waves without generating additional EM waves with active RF chains. Our rate analysis in the large reflective element regime reveals that our lower and upper bounds for the achievable rate are asymptotically exact. Moreover, in the asymptotic

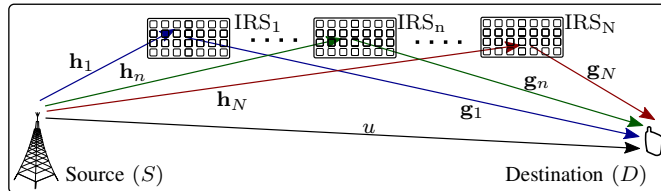


Fig. 1. System model - a distributed IRS-aided communication set-up.

operating regime, the transmit power can be scaled inversely proportional to the square of number of reflective elements at an IRS, while achieving a finite asymptotic rate. The accuracy of our analysis is verified via Monte-Carlo simulations, and a set of rigorous numerical results is presented to investigate the performance of the distributed IRS-aided communication system. Our results reveal that a distributed deployment of IRS can be exploited to boost the outage, average SER performances, and achievable rate compared to the direct transmission and single IRS-aided set-ups.

**Notation:**  $\mathbf{x}^T$  denotes the transpose of  $\mathbf{x}$ .  $\mathbb{E}[X]$  and  $\text{Var}[X]$  represent the expectation and variance of a random variable (RV)  $X$ , respectively.  $X \sim \mathcal{N}(\mu_X, \sigma_X^2)$  denotes that  $X$  is Gaussian distributed with  $\mu_X$  mean and  $\sigma_X^2$  variance.  $\mathcal{O}(\cdot)$  denotes the higher order terms of the MacLaurin series expansion [25, Eq. (0.318.2)].  $\mathcal{Q}(\cdot)$  is the Gaussian- $\mathcal{Q}$  function [26],  $\Gamma(t)$  is the Gamma function [25, Eq. (8.310.1)],  $\Gamma(\alpha, x)$  is the upper incomplete Gamma function [25, Eq. (8.350.2)], and  $\gamma(\alpha, x)$  denotes the lower incomplete Gamma function [25, Eq. (8.350.1)]. Moreover,  $\mathcal{K}_\nu(\cdot)$  represents the modified Bessel function of the second kind [25, Eq. (8.407)] and  $F(\cdot, \cdot; \cdot; \cdot)$  is the Gauss Hypergeometric function [25, Eq. (9.100)].

## II. SYSTEM, CHANNEL AND SIGNAL MODELS

### A. System and channel model

We consider a distributed IRS-assisted wireless communication network having a single-antenna source ( $S$ ), a single-antenna destination ( $D$ ), and  $N$  distributed IRSs with  $L$  passive reflective elements at each IRS (see Fig. 1). The  $S$  serves  $D$  through  $N$  distributed IRSs and via direct channel. It is assumed that the phase-shifts at the IRS reflective elements can be intelligently controlled such that the received signal at  $D$  can be constructively added.

The reflective channels between  $S$  and the  $l$ th reflective element in the  $n$ th IRS and the  $l$ th reflective element in the  $n$ th IRS and  $D$  are denoted by  $h_{nl}$  and  $g_{nl}$ , respectively. Moreover,  $u$  denotes the direct channel between  $S$  and  $D$ .

All channel envelopes are assumed to be independent Nakagami- $m$  distributed, where  $m$  is the shape parameter. The direct channel ( $u$ ) can be written in its polar form as

$$u = \alpha_u e^{j\theta_u}, \quad (1)$$

where  $\alpha_u$  is the envelope of  $u$  and  $\theta_u$  is the phase of  $u$ . The PDF of  $\alpha_u$  is given by [26]

$$f_{\alpha_u}(x) = \frac{2m_u^{m_u} x^{2m_u-1}}{\Gamma(m_u)\xi_u^{m_u}} \exp\left(\frac{-x^2}{\xi_u}\right), \quad (2)$$

where  $m_u$  is the shape parameter and  $\xi_u = m_u \zeta_u$  is the scaling parameter. Here,  $\zeta_u$  accounts for the large-scale fading/path-loss of the channel. Similarly, the  $S$ -to-IRS and IRS-to- $D$  channels can be defined as

$$v_{nl} = \alpha_{v_{nl}} e^{j\theta_{v_{nl}}}, \quad (3)$$

where  $v \in \{h, g\}$ . Moreover,  $\alpha_{v_{nl}}$  is the envelope of  $v_{nl}$  and  $\theta_{v_{nl}}$  is the phase. Then, the PDF of  $\alpha_{v_{nl}}$  is given as follows:

$$f_{\alpha_{v_{nl}}}(x) = \frac{2m_v^{m_v} x^{2m_v-1}}{\Gamma(m_v)\xi_{v_n}^{m_v}} \exp\left(\frac{-x^2}{\xi_{v_n}}\right), \quad (4)$$

where  $m_{v_{nl}} = m_v$  and  $\xi_{v_{nl}} = m_{v_{nl}} \zeta_{v_{nl}} = \xi_{v_n}$  are the shape and scaling parameters, respectively. Here, it is assumed that large-scale fading parameters are the same for a given IRS because its reflective elements are co-located;  $\xi_{v_{nl}} = \xi_{v_n}, \forall l$ . However,  $\xi_{v_n}$  depends on the IRS index ( $n$ ) because geographically distributed IRS deployment.

## B. Signal model

The signal transmitted by  $S$  reaches at  $D$  through the reflected channels of  $N$  distributed IRSs and the direct channel. The signal received at  $D$  can be written as

$$r = \sqrt{P} \left( u + \sum_{n=1}^N \mathbf{g}_n^T \Theta_n \mathbf{h}_n \right) x + w, \quad (5)$$

where  $x$  is the transmitted signal at  $S$  satisfying  $\mathbb{E}[|x|^2] = 1$ ,  $P$  is the transmit power, and  $w$  is an additive white Gaussian noise (AWGN) at  $D$  having zero mean and variance of  $\sigma_w^2$  such that  $w \sim \mathcal{CN}(0, \sigma_w^2)$ . In (5),  $\mathbf{h}_n = [h_{n1}, \dots, h_{nl}, \dots, h_{nL}]^T \in \mathbb{C}^{L \times 1}$  is the channel vector between  $S$  and the  $n$ th IRS and  $\mathbf{g}_n^T = [g_{n1}, \dots, g_{nl}, \dots, g_{nL}] \in \mathbb{C}^{1 \times L}$  accounts for the channel vector between the  $n$ th IRS and  $D$ . Moreover,  $\Theta_n = \text{diag}(\eta_{n1} e^{j\theta_{n1}}, \dots, \eta_{nl} e^{j\theta_{nl}}, \dots, \eta_{nL} e^{j\theta_{nL}}) \in \mathbb{C}^{L \times L}$  is a diagonal matrix, which captures the reflection properties of the  $n$ th IRS. Here,  $\eta_{nl} e^{j\theta_{nl}}$  is a complex-valued reflection coefficient at the  $l$ th reflective element of the  $n$ th IRS, where  $\eta_{nl}$  and

$\theta_{nl}$  are the magnitude of attenuation and phase-shift, respectively. Thus, the signal received at  $D$  in (5) can be rewritten as

$$r = \sqrt{P} \left( u + \sum_{n=1}^N \sum_{l=1}^L g_{nl} \eta_{nl} e^{j\theta_{nl}} h_{nl} \right) x + w. \quad (6)$$

The SNR at  $D$  can be derived via (6) as

$$\gamma = \bar{\gamma} \left| u + \sum_{n=1}^N \sum_{l=1}^L g_{nl} \eta_{nl} e^{j\theta_{nl}} h_{nl} \right|^2, \quad (7)$$

where  $\bar{\gamma} = P/\sigma_w^2$  is the transmit SNR. Then, by substituting (1) and (3) into (7), this SNR can be written in terms of the channel phases as

$$\gamma = \bar{\gamma} \left| \alpha_u e^{j\theta_u} + \sum_{n=1}^N \sum_{l=1}^L \eta_{nl} \alpha_{g_{nl}} \alpha_{h_{nl}} e^{j(\theta_{nl} + \theta_{g_{nl}} + \theta_{h_{nl}})} \right|^2. \quad (8)$$

This analysis (8) reveals that the received SNR at  $D$  can be maximized when  $NL$  signal terms inside the summation of (8) are constructively added to the signal component received via the direct channel. By controlling the phase-shifts at each IRS reflective element ( $\theta_{nl}$ ), the phases inside the double summation in (8) can be adjusted to enable a constructive addition of the received signal components via the direct and reflected channels. Thus, the optimal choice of  $\theta_{nl}$  to maximize the received SNR at  $D$  can be given by [9]

$$\theta_{nl}^* = \operatorname{argmax}_{-\pi \leq \theta_{nl} \leq \pi} \gamma = \theta_u - (\theta_{g_{nl}} + \theta_{h_{nl}}), \quad (9)$$

for  $n \in \{1, \dots, N\}$  and  $l \in \{1, \dots, L\}$ . By using (9), the optimal SNR at  $D$  can be derived as

$$\gamma^* = \bar{\gamma} \left[ \alpha_u + \sum_{n=1}^N \sum_{l=1}^L \eta_{nl} \alpha_{g_{nl}} \alpha_{h_{nl}} \right]^2. \quad (10)$$

### III. PERFORMANCE ANALYSIS

#### A. Statistical characterization of the optimal received SNR

The  $\alpha_{g_{nl}}$  and  $\alpha_{h_{nl}}$  in (10) for  $n \in \{1, \dots, N\}$  and  $l \in \{1, \dots, L\}$  are independently distributed Nakagami RVs, and hence, the exact derivations of the PDFs of

$$Y = \sum_{n=1}^N \sum_{l=1}^L \eta_{nl} \alpha_{g_{nl}} \alpha_{h_{nl}} \quad \text{and} \quad \gamma^* = \bar{\gamma} \underbrace{[\alpha_u + Y]}_R^2 = \bar{\gamma} R^2, \quad (11)$$

seem mathematically involved and may not provide useful design insights. Nevertheless, even for moderately large values of the product  $NL$ ,  $Y$  can be tightly approximated by an one-sided

Gaussian distributed random variable ( $\tilde{Y}$ ) by invoking the CLT [26]. Then, an approximated PDF for  $Y$  can be written as (see Appendix A)

$$f_Y(y) \approx f_{\tilde{Y}}(y) = \begin{cases} \frac{\psi}{\sqrt{2\pi\sigma_Y^2}} \exp\left(-\frac{(y-\mu_Y)^2}{2\sigma_Y^2}\right), & y \geq 0, \\ 0, & y < 0, \end{cases} \quad (12)$$

where  $\psi \triangleq 1/\mathcal{Q}(-\mu_Y/\sigma_Y)$  is a normalization factor to satisfy  $\int_{-\infty}^{\infty} f_{\tilde{Y}}(x)dx = 1$ , and  $\mathcal{Q}(\cdot)$  is the Gaussian- $\mathcal{Q}$  function [26]. In (12),  $\mu_Y$  and  $\sigma_Y^2$  can be derived via the moment matching technique as (see Appendix A)

$$\mu_Y = \sum_{n=1}^N \sum_{l=1}^L \eta_{nl} \sqrt{\frac{\xi_{h_n} \xi_{g_n}}{m_h m_g}} \frac{\Gamma(m_h + 1/2) \Gamma(m_g + 1/2)}{\Gamma(m_h) \Gamma(m_g)}, \quad (13a)$$

$$\sigma_Y^2 = \sum_{n=1}^N \sum_{l=1}^L \eta_{nl}^2 \left( \frac{\xi_{h_n} \xi_{g_n}}{m_h m_g} \right) \frac{\Gamma(m_h + 1) \Gamma(m_g + 1)}{\Gamma(m_h) \Gamma(m_g)} - \mu_Y^2, \quad (13b)$$

where  $\Gamma(t) = \int_0^{\infty} x^t e^{-x} dx$  is the Gamma function [25, Eq. (8.310.1)].

Then, a tight approximation of the PDF of  $R$  in (11) or the exact PDF of its approximation  $\tilde{R} = \alpha_u + \tilde{Y}$  can be derived as (see Appendix B)

$$f_R(x) \approx f_{\tilde{R}}(x) = \lambda e^{-\Delta \left( \frac{x-\mu_Y}{2\sigma_Y^2 \sqrt{a}} \right)^2} \sum_{k=0}^{2m_u-1} \binom{2m_u-1}{k} \left( \frac{x-\mu_Y}{2\sigma_Y^2 \sqrt{a}} \right)^{2m_u-1-k} \left[ \Gamma\left( \frac{k+1}{2}, \left( \frac{x-\mu_Y}{2\sigma_Y^2 \sqrt{a}} \right)^2 \right) \right], \quad (14)$$

where  $\Gamma(\alpha, x) = \int_x^{\infty} e^{-t} t^{\alpha-1} dt$  is the upper incomplete Gamma function [25, Eq. (8.350.2)].

Here,  $a$ ,  $\lambda$ , and  $\Delta$  are given by

$$a = \frac{m_u}{\xi_u} + \frac{1}{2\sigma_Y^2}, \quad \text{and} \quad \lambda = \frac{m_u^{m_u} \psi}{\Gamma(m_u) \xi_u^{m_u} a^{m_u} \sqrt{2\pi\sigma_Y^2}}, \quad (15a)$$

$$\Delta = \left( \frac{1}{2\sigma_Y^2} - \frac{1}{4a\sigma_Y^4} \right) 4\sigma_Y^4 a. \quad (15b)$$

Via  $\tilde{R} = \alpha_u + \tilde{Y}$  in (14), a tight approximation to the optimal SNR ( $\gamma^*$ ) can be written as

$$\gamma^* \approx \tilde{\gamma}^* = \bar{\gamma} \tilde{R}^2. \quad (16)$$

Then, an approximation for the PDF of  $\gamma^* = \bar{\gamma} R^2$  or the exact PDF of  $\tilde{\gamma}^* = \bar{\gamma} \tilde{R}^2$  in (16) can be derived by using (14) as [26]

$$f_{\gamma^*}(y) \approx f_{\tilde{R}}\left(\sqrt{y/\bar{\gamma}}\right) \times \frac{1}{2\sqrt{\bar{\gamma}y}}. \quad (17)$$

Next, the CDF of  $\tilde{R}$  can be derived as (see Appendix C)

$$F_{\tilde{R}}(x) = 1 - \int_x^{\infty} f_{\tilde{R}}(u) du = 1 - \frac{\lambda}{2a^{m_u}} \sum_{k=0}^{2m_u-1} \binom{2m_u-1}{k} I_k, \quad (18)$$



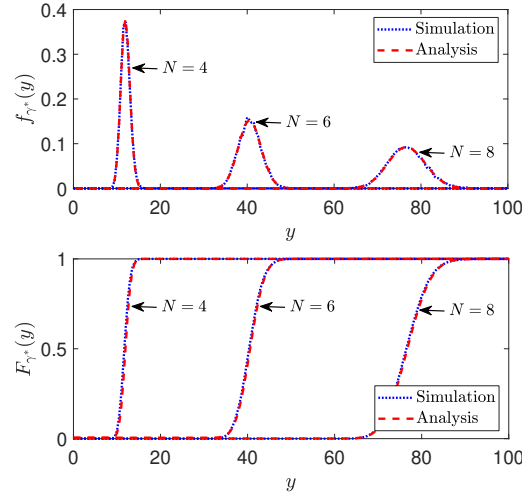


Fig. 2. The PDF and CDF of the received SNR ( $\gamma^*$ ) for  $N \in \{4, 6, 8\}$ ,  $L = 32$ ,  $m_u = m_h = m_g = 3$ , and  $\bar{\gamma} = -10\text{dB}$ .

where  $I_k$  is given as

$$I_k = \begin{cases} I_k^o, & \text{odd } k, \\ I_k^e, & \text{even } k. \end{cases} \quad (19)$$

In (19),  $I_k^o$  is given by

$$I_k^o = \begin{cases} \frac{q(\gamma_o-1)!}{2} \sum_{i=0}^{\gamma_o-1} \frac{(\Delta+1)^{k/2-m_u-i}}{i!} (2\Gamma(m_u + i + k/2) \\ - \Gamma(m_u + i - k/2, (\Delta+1)l_{min}^2)), & \text{for } x < \mu_Y, \\ \frac{q(\gamma_o-1)!}{2} \sum_{i=0}^{\gamma_o-1} \frac{(\Delta+1)^{k/2-m_u-i}}{i!} \Gamma(m_u + i - k/2, (\Delta+1)l_{min}^2), & \text{for } x > \mu_Y, \end{cases} \quad (20)$$

where  $q = 2\sigma_Y^2\sqrt{a}$ ,  $\gamma_o = (k+1)/2$ , and  $l_{min} = (x - \mu_Y)/q$ . Here,  $I_k^e$  in (19) can be given as

$$I_k^e = \frac{q(\gamma_e-1)!}{2} \sum_{j=0}^{\gamma_e-1} \frac{\Delta^{j-\gamma_e}}{j!} \left( \Gamma\left(\frac{k+1}{2}, l_{min}^2\right) l_{min}^{2j} e^{-\Delta l_{min}^2} - \frac{\Gamma\left(j + \frac{k}{2} + \frac{1}{2}, (\Delta+1)l_{min}^2\right)}{(\Delta+1)^{j+\frac{k}{2}+\frac{1}{2}}} \right), \quad (21)$$

where  $\gamma_e = m - k/2$ . Then, the CDF of  $\gamma^* = \bar{\gamma}R^2$  can be approximated as [26]

$$F_{\gamma^*}(y) = \Pr(\gamma^* \leq y) \approx F_{\bar{R}}\left(\sqrt{y/\bar{\gamma}}\right). \quad (22)$$

**Remark 1:** The accuracy of the approximated PDF and CDF of  $\gamma^*$  is verified by plotting (17), (22) and the Monte-Carlo simulations of the exact counterparts in Fig. 2 and Fig. 3 for different  $N$  and  $L$ . Fig. 2 and Fig. 3 reveal that our analytical approximations for the PDF (17) and CDF (22) of  $\gamma^*$  are accurate even for moderately large number of reflective elements ( $L$ ) at the IRS. Since IRSs are typically made of cost-effective reflective elements [27], a moderately large  $N$  is practically feasible.

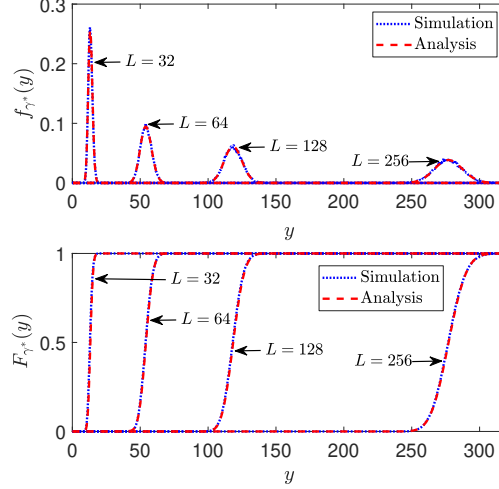


Fig. 3. The PDF and CDF of the received SNR ( $\gamma^*$ ) for  $N = 2$ ,  $L \in \{32, 64, 128, 256\}$ ,  $m_u = m_h = m_g = 3$ , and  $\bar{\gamma} = -10$  dB.

### B. Kullback-Leibler (KL) divergence

In this section, the accuracy of our statistical characterization of the received SNR in Section III-A is investigated by using the KL divergence [28], [29]. Specifically, we analytically quantify the KL divergence between the exact PDF of  $z_{nl} = \alpha_{h_{nl}}\alpha_{g_{nl}}$  and its approximated PDF as one-sided Gaussian distribution (12). Thus, the KL divergence can be defined as [28], [29]

$$\mathcal{D}_{KL} = \mathbb{E} \left[ \log \left( \frac{f_{z_{nl}}^{exact}(x)}{f_{z_{nl}}^{app}(x)} \right) \right], \quad (23)$$

where the expectation is taken with respect to the exact PDF of  $z_{nl}$ . The exact PDF of  $z_{nl}$  is given as (see Appendix A)

$$f_{z_{nl}}^{exact}(x) = \alpha' x^{m_h+m_g-1} \mathcal{K}_{m_h-m_g} \left( 2x \sqrt{\frac{m_h m_g}{\xi_{h_n} \xi_{g_n}}} \right), \quad x \geq 0, \quad (24)$$

where  $\alpha'$  is given in (55b). The approximated PDF of  $z_{nl}$  can be derived via (12) as

$$f_{z_{nl}}^{app}(x) = \frac{\psi_{z_{nl}}}{\sqrt{2\pi\sigma_{z_{nl}}^2}} \exp \left( -\frac{(x - \mu_{z_{nl}})^2}{2\sigma_{z_{nl}}^2} \right), \quad x \geq 0, \quad (25)$$

where  $\psi_{z_{nl}} \triangleq 1/\mathcal{Q}(-\mu_{z_{nl}}/\sigma_{z_{nl}})$  is a normalization factor. Moreover,  $\mu_{z_{nl}}$  and  $\sigma_{z_{nl}}^2$  are given as (see Appendix A)

$$\mu_{z_{nl}} = \sqrt{\frac{\xi_{h_n} \xi_{g_n}}{m_h m_g}} \frac{\Gamma(m_h + 1/2) \Gamma(m_g + 1/2)}{\Gamma(m_h) \Gamma(m_g)}, \quad (26a)$$

$$\sigma_{z_{nl}}^2 = \left( \frac{\xi_{h_n} \xi_{g_n}}{m_h m_g} \right) \frac{\Gamma(m_h + 1) \Gamma(m_g + 1)}{\Gamma(m_h) \Gamma(m_g)} - \mu_{z_{nl}}^2. \quad (26b)$$

Then, the KL divergence can be given as

$$\mathcal{D}_{KL} = F + \mathbb{E} [\log (x^{m_h+m_g-1})] + \mathbb{E} \left[ \log \left( \mathcal{K}_{m_h-m_g} \left( 2x \sqrt{\frac{m_h m_g}{\xi_{h_n} \xi_{g_n}}} \right) \right) \right] + \mathbb{E} \left[ \frac{(x - \mu_{z_{nl}})^2}{2\sigma_{z_{nl}}^2} \right], \quad (27)$$

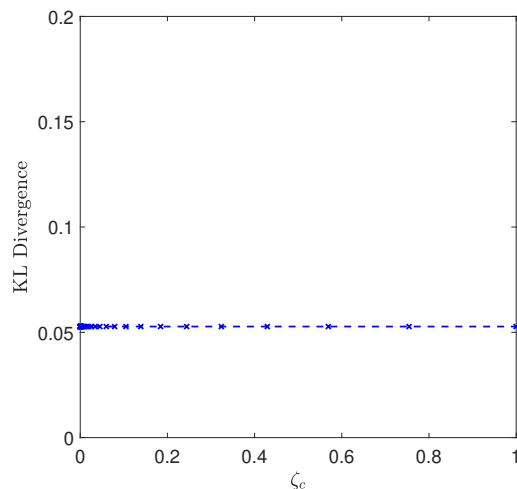


Fig. 4. The KL divergence of the approximated PDF of  $z_{nl}$  for  $m_h = m_g = 3$ .

where  $F = \log(\alpha') - \log(\psi_{z_{nl}}/\sqrt{2\pi\sigma_{z_{nl}}^2})$ .

**Remark 2:** In Fig. 4, the KL divergence of the approximated PDF of  $z_{nl}$  is plotted as a function of  $\zeta_c = \xi_{h_{nl}}/m_h = \xi_{g_{nl}}/m_g$ . Since  $\zeta_c$  accounts for the large-scale fading, the range of  $\zeta_c$  is set to  $(0, 1)$ . Fig. 4 clearly shows that the KL divergence of the approximated PDF is as low as  $\mathcal{D}_{KL} \approx 5.2 \times 10^{-2}$  for the entire range of  $\zeta_c$ . This observation thus validates the tightness of our approximated PDF of the received optimal SNR to the exact counterpart.

### C. Outage probability

The probability that the instantaneous SNR falls below a threshold SNR ( $\gamma_{th}$ ) is defined as the SNR outage probability, and a tight approximation to it can be obtained via (22) as

$$P_{out} = P_r(\gamma \leq \gamma_{th}) \approx F_{\gamma^*}(\gamma_{th}). \quad (28)$$

### D. Average achievable rate

The average achievable rate can be defined as follows:

$$\mathcal{R} = \mathbb{E}[\log_2(1 + \gamma^*)]. \quad (29)$$

Since the exact derivation of  $\mathcal{R}$  in (29) seems mathematically intractable, we resort to tight upper and lower bounds by invoking the Jensen's inequality as [30]

$$\mathcal{R}_{lb} \leq \mathcal{R} \leq \mathcal{R}_{ub}. \quad (30)$$

In (30),  $\mathcal{R}_{lb}$  and  $\mathcal{R}_{ub}$  are defined as

$$\mathcal{R}_{lb} = \log_2(1 + (\mathbb{E}[1/\gamma^*])^{-1}) \approx \log_2(1 + (\mathbb{E}[1/\tilde{\gamma}^*])^{-1}), \quad (31a)$$

$$\mathcal{R}_{ub} = \log_2(1 + \mathbb{E}[\gamma^*]) \approx \log_2(1 + \mathbb{E}[\tilde{\gamma}^*]). \quad (31b)$$

The expectation term in (31b) can be approximately derived as (see Appendix D-A)

$$\mathbb{E}[\gamma^*] \approx \mathbb{E}[\tilde{\gamma}^*] = \bar{\gamma} (\sigma_u^2 + \sigma_Y^2 + 2\mu_u\mu_Y + \mu_u^2 + \mu_Y^2), \quad (32)$$

where  $\mu_Y$  and  $\sigma_Y^2$  are defined in (13a) and (13b), respectively. In (32),  $\mu_u$  and  $\sigma_u^2$  are defined as

$$\mu_u = \frac{\Gamma(m_u + 1/2)}{\Gamma(m_u)} \left( \frac{\xi_u}{m_u} \right)^{1/2}, \quad (33a)$$

$$\sigma_u^2 = \xi_u \left( 1 - \frac{1}{m_u} \left( \frac{\Gamma(m_u + 1/2)}{\Gamma(m_u)} \right)^2 \right). \quad (33b)$$

Next, the expectation term in (31a) can be computed as

$$\mathbb{E}[1/\gamma^*] \approx \mathbb{E}[1/\tilde{\gamma}^*] = \frac{1}{\mathbb{E}[\tilde{\gamma}^*]} + \frac{\text{Var}[\tilde{\gamma}^*]}{(\mathbb{E}[\tilde{\gamma}^*])^3}, \quad (34)$$

where  $\mathbb{E}[\tilde{\gamma}^*]$  is defined in (32). Here,  $\text{Var}[\tilde{\gamma}^*]$  is derived as (see Appendix D-B)

$$\text{Var}[\tilde{\gamma}^*] = \bar{\gamma}^2 \mathbb{E}[\tilde{R}^4] - (\mathbb{E}[\tilde{\gamma}^*])^2, \quad (35)$$

where  $\mathbb{E}[\tilde{R}^4]$  is given by

$$\mathbb{E}[\tilde{R}^4] = \sum_{n=0}^4 \binom{4}{n} \mathbb{E}[\alpha_u^{(4-n)}] \mathbb{E}[\tilde{Y}^n]. \quad (36)$$

Here,  $\mathbb{E}[\alpha_u^n]$  for  $n \in \{1, 2, 3, 4\}$  can be derived as

$$\mathbb{E}[\alpha_u^n] = \frac{\Gamma(m_u + n/2)}{\Gamma(m_u)} \left( \frac{\xi_u}{m_u} \right)^{n/2}. \quad (37)$$

Moreover,  $\mathbb{E}[\tilde{Y}^n]$  for  $n \in \{1, 2, 3, 4\}$  is given by

$$\mathbb{E}[\tilde{Y}^n] = \frac{\psi}{2\sqrt{\pi}} \sum_{i=0}^n \binom{n}{i} \left( \sqrt{2\sigma_Y^2} \right)^{n-i} \mu_Y^i I\left(n-i, \frac{-\mu_Y}{2\sigma_Y^2}\right), \quad (38)$$

where  $I(\cdot, \cdot)$  is given as

$$I(m, t) = \begin{cases} (-1)^m \gamma\left(\frac{m+1}{2}, t^2\right) + \Gamma\left(\frac{m+1}{2}\right), & \text{for } t \leq 0, \\ \Gamma\left(\frac{m+1}{2}, t^2\right), & \text{otherwise,} \end{cases} \quad (39)$$

where  $\gamma(\alpha, x) = \int_0^x e^{-t} t^{\alpha-1} dt$  is the lower incomplete Gamma function [25, Eq. (8.350.1)].

Finally,  $\mathcal{R}_{lb}$  and  $\mathcal{R}_{ub}$  can be derived as

$$\mathcal{R}_{lb} = \log_2 \left( 1 + \frac{\bar{\gamma} (\sigma_u^2 + \sigma_Y^2 + 2\mu_u\mu_Y + \mu_u^2 + \mu_Y^2)^3}{\sum_{n=0}^4 \binom{4}{n} \frac{\Gamma(m_u + \frac{(4-n)}{2})}{\Gamma(m_u)} \left( \frac{\xi_u}{m_u} \right)^{(4-n)/2} \frac{\psi}{2\sqrt{\pi}} \sum_{i=0}^n \binom{n}{i} (2\sigma_Y^2)^{(n-i)/2} \mu_Y^i I\left(n-i, \frac{-\mu_Y}{2\sigma_Y^2}\right)} \right), \quad (40)$$

$$\mathcal{R}_{ub} = \log_2 \left( 1 + \bar{\gamma} (\sigma_u^2 + \sigma_Y^2 + 2\mu_u\mu_Y + \mu_u^2 + \mu_Y^2) \right), \quad (41)$$

where  $\sigma_u^2$ ,  $\sigma_Y^2$ ,  $\mu_u$ , and  $\mu_Y$  are defined in (33b), (13b), (33a), and (13a), respectively.

1) *Asymptotic achievable rate as the number of IRS elements grows large ( $L \rightarrow \infty$ ):* To obtain further insights, the asymptotic achievable rate can be derived as the number of IRS elements grows without bound ( $L \rightarrow \infty$ ). In this operating regime, we observe that the transmit power can be scaled inversely proportional to the square of the number of IRS elements:  $\lim_{L \rightarrow \infty} P = P_E/L^2$ . By using this transmit power scaling law, the lower and upper rate bounds in (40) and (41), respectively, can be shown to approach an asymptotic limit as follows (see Appendix D-C):

$$\lim_{L \rightarrow \infty} \mathcal{R}_{lb} \rightarrow \mathcal{R}^\infty, \quad \text{and} \quad \lim_{L \rightarrow \infty} \mathcal{R}_{ub} \rightarrow \mathcal{R}^\infty, \quad (42)$$

where the asymptotic achievable rate  $\mathcal{R}^\infty$  in large  $L$  regime is given by

$$\lim_{L \rightarrow \infty} \mathcal{R} \rightarrow \mathcal{R}^\infty = \log_2 \left( 1 + \bar{\gamma}_E \left( \sum_{n=1}^N \eta_n \sqrt{\frac{\xi_{h_n} \xi_{g_n}}{m_h m_g} \frac{\Gamma(m_h + 1/2) \Gamma(m_g + 1/2)}{\Gamma(m_h) \Gamma(m_g)}} \right)^2 \right), \quad (43)$$

where  $\bar{\gamma}_E = P_E/\sigma_w^2$  and  $\eta_n = \eta_{nl}$ ,  $\forall n$ .

**Remark 3:** Our asymptotic analysis reveals that our lower (40) and upper (41) rate bounds converge to a common limit, and hence, these rate bounds are asymptotically exact in large  $L$  regime. Moreover, the transmit power at  $S$  can be scaled inversely proportional to  $L^2$ , while achieving a finite rate at  $D$ .

### E. Average symbol error rate (SER)

The average SER can be defined as the expectation of conditional error probability ( $P_{e|\gamma^*}$ ) over the probability distribution of  $\gamma^*$  [31]. For a wide-range of coherent modulation schemes,  $P_{e|\gamma^*}$  is given by [31]

$$P_{e|\gamma^*} = \omega \mathcal{Q} \left( \sqrt{\vartheta \gamma^*} \right), \quad (44)$$

where  $\omega$  and  $\vartheta$  depend on the modulation scheme [31]. For instance, the pair of parameters  $(\omega, \vartheta)$  for binary phase-shift keying (BPSK) and quadrature phase-shift keying (QPSK) are given by  $(\omega = 1, \vartheta = 2)$  and  $(\omega = 2, \vartheta = 1)$ , respectively [31]. Then, the average SER can be defined as

$$\bar{P}_e = \mathbb{E} \left[ \omega \mathcal{Q} \left( \sqrt{\vartheta \gamma^*} \right) \right]. \quad (45)$$

Then, by using  $\tilde{\gamma}^*$  in (16), a tight approximation for the average SER can be derived as

$$\bar{P}_e \approx \tilde{P}_e = \omega \mathbb{E}_{\alpha_u} \left[ \mathbb{E}_{\tilde{Y}} \left[ \mathcal{Q} \left( \vartheta_b (\alpha_u + \tilde{Y}) \right) \right] \right], \quad (46)$$

where  $\vartheta_b = \sqrt{\vartheta\bar{\gamma}}$ . Then, a tight approximation to the average SER  $\tilde{P}_e$  can be derived as (see Appendix E)

$$\tilde{P}_e \approx \omega B \sum_{k=0}^{2m_u-1} \left( \frac{-u_1}{2v_1} \right)^{2m_u-1-k} \Gamma(\gamma_b) \sum_{i=0}^{\gamma_b-1} \frac{v_1^{i-\gamma_b}}{i!} \left( \mathcal{Q}(\sqrt{2}r) \left( \frac{u_1}{2v_1} \right)^{2i} - \frac{se^{\frac{u_2^2}{4v_2} - \frac{u_1^2}{4v_1} - r}}{\sqrt{\pi}} \sum_{j=0}^{2i} q_b^{2i-j} I_b \right), \quad (47)$$

where  $\gamma_b = (k+1)/2$ ,  $q_b = u_1/2v_1 - u_2/2v_2$ , and  $I_b$  is defined as

$$I_b = \frac{v_2^{(j+1)/2}}{2} \begin{cases} \Gamma\left(\frac{j+1}{2}, \frac{u_2^2}{4v_2}\right), & \text{for } \frac{u_2}{2v_2} > 0, \\ (-1)^j \gamma\left(\frac{j+1}{2}, \frac{u_2^2}{4v_2}\right) + \Gamma\left(\frac{j+1}{2}\right), & \text{otherwise.} \end{cases} \quad (48)$$

Moreover,  $B$ ,  $s$ ,  $r$ , and  $\{u_i, v_i\}$  for  $i \in \{1, 2\}$  are defined as follows:

$$B = \frac{m_u^{m_u} \psi \exp\left(\frac{u_1^2}{4v_1} - \frac{\mu_Y^2}{2\sigma_Y^2} - \frac{1}{4a_1} \left(d\vartheta_b - \frac{\mu_Y}{\sigma_Y}\right)^2\right)}{2\Gamma(m_u) \xi_u^{m_u} \sqrt{2\pi\sigma_Y^2 a_1}}, \quad (49a)$$

$$s = \frac{c\vartheta_b^2}{2\sqrt{a_1}}, \quad (49b)$$

$$r = \frac{1}{2\sqrt{a_1}} \left(d\vartheta_b - \frac{\mu_Y}{\sigma_Y}\right), \quad (49c)$$

$$u_1 = d\vartheta_b - \frac{c\vartheta_b^2}{a_1} \left(d\vartheta_b - \frac{\mu_Y}{\sigma_Y}\right), \quad (49d)$$

$$u_2 = u_1 + 2sr, \quad (49e)$$

$$v_1 = c\vartheta_b - \frac{c^2\vartheta_b^2}{a_1} + \frac{m_u}{\xi_u}, \quad (49f)$$

$$v_2 = v_1 + s^2, \quad (49g)$$

where  $a_1 = c\vartheta_b^2 + 1/2\sigma_Y^2$ ,  $c = 0.374$ , and  $d = 0.777$  [32].

### F. Achievable diversity order

The diversity order is defined as the negative slope of the average SER or outage probability versus the average SNR curve plotted in a log-log scale in the high SNR regime [33], and it can be defined as

$$G_d = - \lim_{\bar{\gamma} \rightarrow \infty} \frac{\log(\bar{P}_e)}{\log(\bar{\gamma})} = - \lim_{\bar{\gamma} \rightarrow \infty} \frac{\log(P_{out})}{\log(\bar{\gamma})}. \quad (50)$$

The diversity order provides insights on how the outage probability or average SER decays with the average SNR. Thus, in this subsection, we derive the asymptotic outage probability and the average SER in the high SNR regime, and thereby, the achievable diversity order and array/coding gain are quantified.

1) *Asymptotic outage probability*: The outage probability can be asymptotically approximated in the high SNR regime as [33]

$$\lim_{\bar{\gamma} \rightarrow \infty} P_{out} = P_{out}^{\infty} \approx O_c \left( \frac{\gamma_{th}}{\bar{\gamma}} \right)^{G_d} + \mathcal{O}(\bar{\gamma}^{-(G_d+1)}), \quad (51)$$

where  $O_c$  is a measure of the array/coding gain and  $G_d$  is the diversity order [33]. Then, an asymptotic approximation for  $P_{out}$  can be derived as (see Appendix F)

$$P_{out}^{\infty} = \Omega \Phi(N, L) \left( \frac{\gamma_{th}}{\bar{\gamma}} \right)^{G_d} + \mathcal{O}(\bar{\gamma}^{-(G_d+1)}), \quad (52)$$

where the diversity order ( $G_d$ ) is given by

$$G_d = NL \min(m_h, m_g) + m_u. \quad (53)$$

Moreover, in (52),  $\Omega$  and  $\Phi(N, L)$  are defined as

$$\Omega = \frac{2m_u^{m_u} \Gamma(2m_u)}{2G_d \Gamma(m_u) \xi_u^{m_u} \Gamma(2G_d)}, \quad \text{and} \quad \Phi(N, L) = \prod_{n=1}^N \prod_{l=1}^L \eta_{nl} \theta_n, \quad (54)$$

where

$$\theta_n = \alpha' \pi \left( 4 \sqrt{\frac{m_s m_l}{\xi_{s_n} \xi_{l_n}}} \right)^{(m_s - m_l)} \frac{\Gamma(2m_s) \Gamma(2m_s - 2m_l)}{\Gamma(m_l - m_s + 1/2)}, \quad (55a)$$

$$\alpha' = \frac{4}{\Gamma(m_s) \Gamma(m_l)} \left( \frac{m_s m_l}{\xi_{s_n} \xi_{l_n}} \right)^{(m_s + m_l)/2}. \quad (55b)$$

Furthermore,  $m_l = \max(m_h, m_g)$  and  $m_s = \min(m_h, m_g)$ . Further,  $\xi_{s_n}$  and  $\xi_{l_n}$  are the scaling parameters related to  $m_s$  and  $m_l$ , respectively, in the Nakagami- $m$  fading channels. Finally,  $O_c$  in (51) can be defined as

$$O_c = \Omega \Phi(N, L). \quad (56)$$

2) *Asymptotic average SER* : Similarly, the average SER can be approximated in the high SNR regime as [33]

$$\lim_{\bar{\gamma} \rightarrow \infty} \bar{P}_e = \bar{P}_e^{\infty} \approx (G_a \bar{\gamma})^{-G_d} + \mathcal{O}(\bar{\gamma}^{-(G_d+1)}), \quad (57)$$

where  $G_d$  and  $G_a$  are diversity order and array gain, respectively. An asymptotic approximation for the average SER (46) in high SNR regime can be derived as (see Appendix F)

$$\bar{P}_e^{\infty} = \left[ (\Lambda \Phi(N, L))^{-\frac{1}{G_d}} \bar{\gamma} \right]^{-G_d} + \mathcal{O}(\bar{\gamma}^{-(G_d+1)}), \quad (58)$$

where  $G_d = m_s NL + m_u$  and  $\Phi(N, L)$  is given in (54). Moreover,  $\Lambda$  is define as

$$\Lambda = \frac{\omega 2^{G_d-1} m_u^{m_u} \Gamma(G_d + 1/2) \Gamma(2m_u)}{\sqrt{\pi} \vartheta^{G_d} G_d \xi_u^{m_u} \Gamma(2G_d) \Gamma(m_u)}. \quad (59)$$

Lastly, the array gain in (57) can be derived as

$$G_a = (\Lambda\Phi(N, L))^{-1/G_a}. \quad (60)$$

**Remark 4:** Our asymptotic performance analysis (53) reveals that the achievable diversity order is a linear function of the number of distributed IRSs and the number of reflective elements in each IRS. It is worth noting that  $S$  and  $D$  are equipped with a single antenna/RF-chain. However, as per analysis, we observe that the distributed IRS deployments can be used to recycle the existing EM waves in the propagation environment without using additional active RF chains to substantially increase the achievable diversity order, and consequently, the system reliability can be boosted in terms of lowering the outage probability and average SER. This is in sharp contrast to the current state-of-the-art in which the diversity order improvements are obtained by virtue of increasing antennas/RF chains at the transmitter/receiver. The proposed distributed IRS-aided system achieves this diversity gain by intelligently controlling the phase-shifts at the distributed passive reflective elements such that the signals received via reflected channels are constructively combined with the direct channel at  $D$ .

#### IV. NUMERICAL RESULTS

In this section, we present our numerical results to investigate the performance gains and to validate our analysis. In our simulations, the large-scale fading is modeled as  $\zeta_{ab} = (d_0/d_{ab})^\nu \times 10^{\varphi_{ab}/10}$ , where  $a \in \{S, n\}$ ,  $b \in \{n, D\}$ ,  $d_{ab}$  is the distance between nodes  $a$  and  $b$ ,  $d_0 = 1$  m is a reference distance,  $\nu = 2.8$  is the path-loss exponent, and  $10^{\varphi_{ab}/10}$  captures log-normal shadow fading with  $\varphi_{ab} \sim (0, 8)$  [34]. In the system topology,  $S$  and  $D$  are in positioned at fixed locations and 1200 m apart from each other. The IRSs are randomly distributed over an area of  $1000 \times 2000$  m<sup>2</sup>. Moreover, the amplitude of reflection coefficients  $\eta_{nl}$  for  $n \in \{1, \dots, N\}$  and  $l \in \{1, \dots, L\}$  is set to 0.9, and unless otherwise specified, the Nakagami- $m$  parameters ( $m_u$ ,  $m_h$ , and  $m_g$ ) are set to 3.

In Fig. 5, we plot the outage probability as a function of the average transmit SNR ( $\bar{\gamma}$ ) by varying the number of distributed IRSs defined by  $N \in \{1, 2, 4, 6, 8\}$ . The exact outage curves are generated by using Monte-Carlo simulation, while the analytical outage curves are plotted via our closed-form derivation in (28). As per Fig. 5, we observe that the tightness of our outage probability approximation significantly improves with  $N$ . Moreover, we observe that the distributed IRS deployment outperforms the single-IRS set-up. For example, the single-IRS



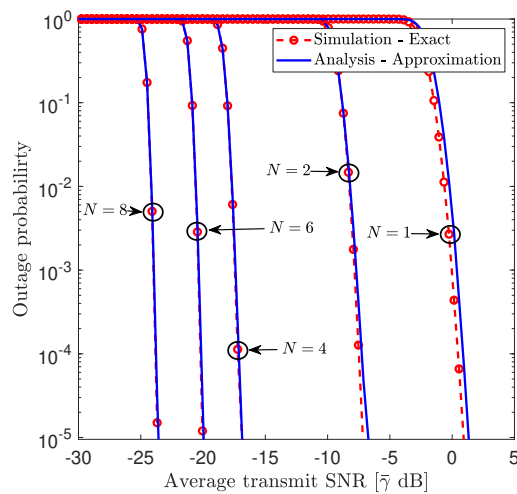


Fig. 5. The outage probability for different number of IRSs in the distributed deployment denoted by  $N \in \{1, 2, 4, 6, 8\}$ , the number of reflective elements per IRS is  $L = 32$ ,  $m_u = m_h = m_g = 3$ , and the threshold SNR is  $\gamma_{th} = 0$  dB.

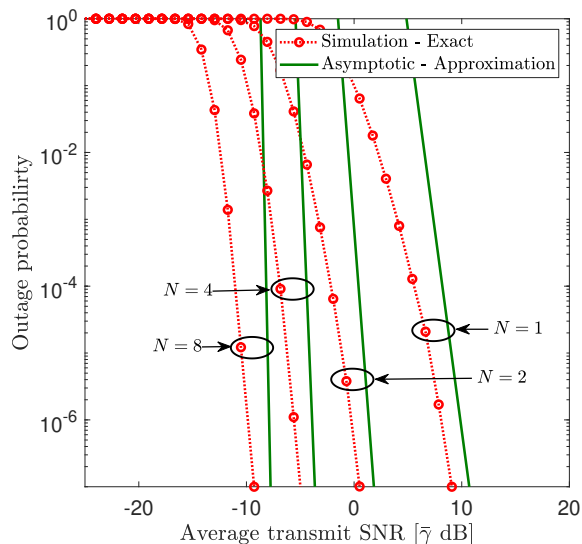


Fig. 6. The outage probability for  $N \in \{1, 2, 4, 8\}$ ,  $L = 6$ ,  $m_u = m_g = 3$ ,  $m_h = 1.5$ , and  $\gamma_{th} = 10$  dB.

deployment requires an average transmit SNR of 1 dB to achieve an outage probability of  $10^{-4}$ , and this is an 104.2% increase compared to the same transmit SNR requirement of the distributed deployment with eight IRS.

In Fig. 6, we investigate asymptotic behavior of the outage probability in the high SNR regime. To this end, our asymptotic outage probability (52) is plotted as a function of the average transmit SNR, and Monte-Carlo simulations are also provided for validation purposes. The asymptotic outage probability curves reveal the achievable diversity orders for different distributed IRS deployments;  $N \in \{1, 2, 4, 8\}$ . For instance, the diversity orders for  $(N = 1, L = 6)$  and  $(N = 2, L = 6)$  cases can be obtained by computing the negative gradients of asymptotic outage curves in Fig. 6 to be 12 and 21, respectively. This observation clearly validates our diversity

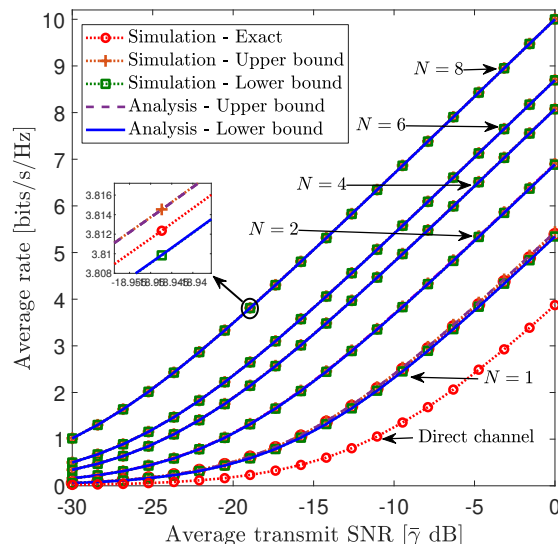


Fig. 7. The average achievable rate for  $N \in \{1, 2, 4, 6, 8\}$ ,  $L = 32$ , and  $m_u = m_h = m_g = 3$ .

order analysis in (53), i.e.,  $G_d = NL \min(m_h, m_g) + m_u$  with  $m_h = 1.5$ ,  $m_g = m_u = 3$ . Thus, the results in Fig. 6 show that the diversity order increases with the number of IRS reflective elements, and consequently, the system reliability can be drastically improved by the proposed distributed IRS-aided system without adopting additional RF chains.

In Fig. 7, we plot the achievable average rate for different number of distributed IRSs as per  $N \in \{1, 2, 4, 6, 8\}$ . The achievable rate lower/upper bounds are plotted via (31a) and (31b), respectively. The accuracy of our rate analysis is also validated via Monte-Carlo simulation of the exact achievable rate. Fig. 7 clearly depicts that our lower/upper bounds are tight even for smaller  $N$ . Fig. 7 reveals that higher the number of distributed IRS, higher the achievable rate. Moreover, Fig. 7 can be used to quantify the rate gains of the distributed IRS deployments compared to the direct transmission. For instance, the single-IRS ( $N = 1$ ) case provides a rate gain of 80.7% compared to the direct transmission at an average transmit SNR of  $-10$  dB. This rate gain increases to 182.5%, 266.2%, and 405.9% for dual-, quadruple-, and octuple-IRS cases, respectively, with respect to the direct channel.

In Fig. 8, the impact of the IRS positions on the average achievable rate is investigated. To this end,  $S$  and  $D$  are in positioned at fixed locations at 500 m apart. The Case-1 plots the achievable rate of the direct channel. For Case-2 and Case-3, the distances between  $S$ -IRS and  $D$ -IRS are 750 m. Moreover, the distances between  $S$ -IRS and  $D$ -IRS for Case-4 and Case-5 are greater than 1600 m. In Case-3 and Case-5, the achievable rates are plotted by assuming that the direct channel in unserviceable and the end-to-end communication is established via the reflected

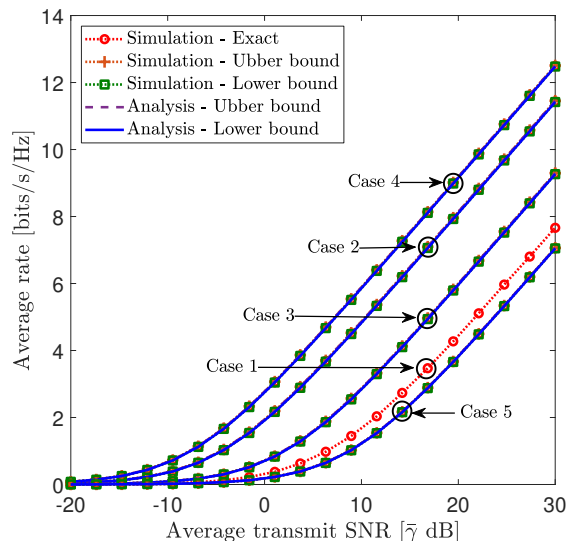


Fig. 8. An average achievable rate comparison for different system configurations. For all cases  $L = 32$  and  $m_u = m_h = m_g = 3$ . The  $N$  for Case-2 to Case-3 are set to  $N = 1$ , whereas for Case-4 to Case-5 are set to  $N = 3$ . These five cases are defined as follows: Case-1: direct channel only, Case-2/Case-3: IRSs are located in closer with/without direct channel, and Case-4/Case-5: IRSs are located far-away and with/without direct channel, respectively.

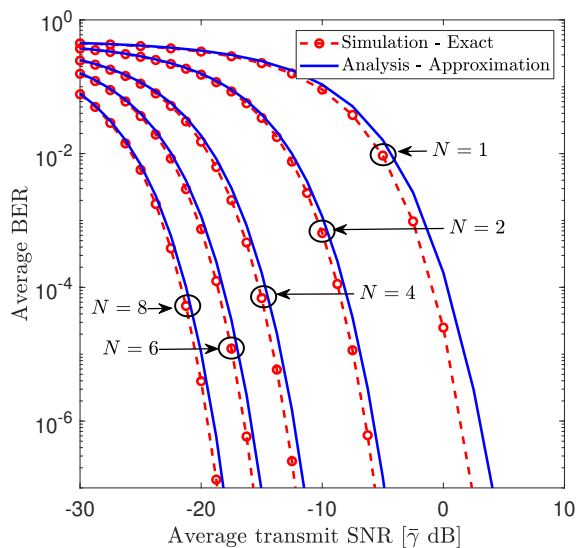


Fig. 9. The average BER of BPSK versus average transmit SNR ( $\bar{\gamma}$ ) for  $N \in \{1, 2, 4, 6, 8\}$ ,  $L = 32$ ,  $m_u = m_h = m_g = 3$ ,  $\omega = 1$ , and  $\vartheta = 2$ .

channels. Fig. 8 shows that the rate of the direct channel is higher than the that of the reflected channels when the IRSs are positioned far away from  $S$  and  $D$  (see Case-1 and Case-5). When comparing Case-2 and Case-3, we can observe that the having the direct channel is beneficial in boosting the achievable rate. Although the IRSs are placed far away in Case-4 than that in Case-3, the achievable rate of the former is higher than that the latter. This is because Case-4 has two additional IRSs than the Case-3. Thus, the distributed IRS deployments can circumvent the rate losses incurred due to larger transmission distances in the reflected channels.

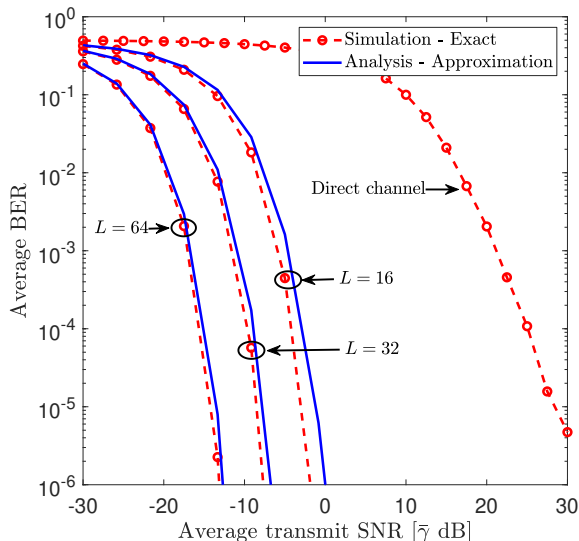


Fig. 10. A comparison of the average BER with/without IRSs for  $N = 2$ ,  $L \in \{16, 32, 64\}$ ,  $m_u = m_h = m_g = 3$ ,  $\omega = 1$ , and  $\vartheta = 2$ .

In Fig. 9, the average bit error rate (BER) of BPSK is plotted against the average transmit SNR ( $\bar{\gamma}$ ) for different number of IRSs;  $N \in \{1, 2, 4, 6, 8\}$ . The exact average BER curves are generated via Monte-Carlo simulations, whereas the analytical curves are plotted by using (47). From Fig. 9, we observe that our average BER analysis in (47) is tight for moderately larger  $NL$  regime. The average BER for a single-IRS set-up is also plotted for the purpose of comparison. Fig. 9 reveals that the distributed IRS deployments outperform the single-IRS set-up. For instance, to achieve an average BER of  $10^{-4}$ , the single-IRS set-up requires an average transmit SNR of 0 dB, which is an 22 dB increase compared to the transmit SNR requirement of the distributed IRS set-up with eight IRSs. Moreover, the achievable average BER significantly decreases when the number of distributed IRSs grows large. For example, at an average SNR of  $-20$  dB, the achievable BER of  $N = 4$  case can be lowered by 99.8% by doubling the number of IRSs to  $N = 8$ .

In Fig. 10, we investigate the effects of increasing number of IRS reflective elements by plotting the average BER of BPSK versus the average SNR. A dual-IRS system is considered and the number of reflective elements is varied as  $L \in \{16, 32, 64\}$ . Analytical average BER is plotted via (47), and it is validated through Monte-Carlo simulations. Fig. 10 shows that the dual-IRS system outperforms the direct channel in terms of the average BER. For example, the direct transmission requires an average SNR of 28 dB to achieve an average BER of  $10^{-5}$ , while this SNR requirement can be lowered by 36 dB with a deployment of a dual-IRS set-up with  $L = 32$ . Moreover, at an average SNR of  $-10$  dB, the average BER can be lowered from

$1.82 \times 10^{-2}$  to  $1.72 \times 10^{-4}$  by doubling the number of reflective elements per IRS from  $L = 16$  case to  $L = 32$  case. Thus, the proposed distributed IRS deployment can be used to significantly boost the reliability of wireless communication systems.

## V. CONCLUSION

In this paper, the fundamental performance metrics of a distributed IRS-aided communication system have been investigated. To this end, the optimal received SNR has been derived by controlling the phase-shifts of the distributed IRS elements. In order to facilitate mathematically tractable performance analysis, this SNR has been statistically characterized by deriving the tight approximations to the PDF and CDF for Nakagami- $m$  fading. The KL divergence has been used to analytically verify the accuracy of our statistical characterization of the received SNR. Thereby, the outage probability, average SER, and achievable rate approximations/bounds have been derived in closed-form. Useful insights on the diversity order and array gain have been drawn by deriving the asymptotic outage probability and the average SER in the high SNR regime. By virtue of an asymptotic achievable rate analysis, it has been shown that the transmit power can be scaled inversely proportional to the square of the number of reflective elements, and in operating regime, our lower and upper rate bounds have been shown to be asymptotically exact. A rigorous set of Monte-Carlo simulations has been presented to validate the accuracy of our analysis. The performance of the proposed distributed IRS-assisted set-up has been compared with a conventional/direct and a single IRS-aided counterparts. Our analysis and numerical results reveal that distributed IRS deployments can be used to significantly enhance the performance of future wireless communications by recycling the existing EM waves via passive IRS reflective elements without generating new EM waves with active RF chains. Thus, the concept distributed IRS-aided communications can be an energy and cost effective paradigm-shift in future wireless designs.

## APPENDIX A

### THE DERIVATION OF $\mu_Y$ IN (13a), $\sigma_Y^2$ IN (13b), AND PDF OF $Y$ IN (12)

First, we define  $Y = \sum_{n=1}^N \sum_{l=1}^L \eta_{nl} z_{nl}$ , where  $z_{nl} = \alpha_{h_{nl}} \alpha_{g_{nl}}$ . Since  $\alpha_{h_{nl}}$  and  $\alpha_{g_{nl}}$  are independent Nakagami- $m$  variables, the PDF of  $z_{nl}$  can be evaluated as

$$\begin{aligned} f_{z_{nl}}(x) &= \int_0^\infty f_{\alpha_{h_{nl}}}(u) f_{\alpha_{g_{nl}}}(x/u) \times \frac{1}{|u|} du = \alpha x^{2m_g-1} \int_0^\infty u^{2(m_h-m_g)-1} e^{-\frac{m_h u^2}{\xi_{h_n}} - \frac{m_g x^2}{\xi_{g_n} u^2}} du \\ &\stackrel{(a)}{=} \frac{\alpha}{2} x^{2m_g-1} \int_0^\infty t^{m_h-m_g-1} e^{-\frac{m_h t}{\xi_{h_n}} - \frac{m_g x^2}{\xi_{g_n} t}} dt \end{aligned}$$

$$\stackrel{(b)}{=} \alpha' x^{m_h+m_g-1} \mathcal{K}_{m_h-m_g} \left( 2x \sqrt{\frac{m_h m_g}{\xi_{h_n} \xi_{g_n}}} \right), \quad (61)$$

where  $\alpha = 4m_h^{m_h} m_g^{m_g} / (\Gamma(m_h)\Gamma(m_g)\xi_{h_n}^{m_h}\xi_{g_n}^{m_g})$  and  $\alpha' = \alpha (m_g \xi_{h_n} / m_h \xi_{g_n})^{(m_h-m_g)/2}$ . Moreover,  $\mathcal{K}_v(\cdot)$  is the Modified Bessel function of second kind [25, Eq. (8.407)]. The step (a) is obtained by letting  $t = u^2$  and the step (b) is computed by using [25, Eq. (3.471.9)]. Then, the  $n$ th moment of  $z_{nl}$  can be derived as follows:

$$\begin{aligned} \mathbb{E}[z_{nl}^n] &= \alpha' \int_0^\infty x^{m_h+m_g+n-1} \mathcal{K}_{m_h-m_g} \left( 2x \sqrt{\frac{m_h m_g}{\xi_{h_n} \xi_{g_n}}} \right) dx \\ &\stackrel{(c)}{=} \frac{\alpha'}{4} \left( \frac{m_h m_g}{\xi_{h_n} \xi_{g_n}} \right)^{\frac{-m_h-m_g-n+1}{2}} \Gamma \left( \frac{2m_h+n}{2} \right) \Gamma \left( \frac{2m_g+n}{2} \right), \end{aligned} \quad (62)$$

where the step (c) is written by using [25, Eq. (6.561.16)]. Then, the mean and the variance of  $Y$  can be given as

$$\mu_Y = \mathbb{E}[Y] = \sum_{n=1}^N \sum_{l=1}^L \eta_{nl} \mathbb{E}[z_{nl}], \quad (63a)$$

$$\sigma_Y^2 = \mathbb{V}\text{ar}[Y] = \sum_{n=1}^N \sum_{l=1}^L \eta_{nl}^2 (\mathbb{E}[z_{nl}^2] - \mathbb{E}[z_{nl}]^2). \quad (63b)$$

By substituting (62) into (63a) and (63b),  $\mu_Y$  and  $\sigma_Y^2$  can be computed as (13a) and (13b), respectively. Then, the PDF of  $Y$  can be approximated by an one-sided Gaussian distribution as given in (12) by invoking the central limit theorem [26].

## APPENDIX B THE DERIVATION OF PDF OF $\tilde{R}$ IN (14)

Since  $\alpha_u$  and  $Y$  are independent RVs, the PDF of  $\tilde{R} = \alpha_u + \tilde{Y}$  can be derived as follows:

$$\begin{aligned} f_{\tilde{R}}(x) &= \int_0^\infty f_u(u) f_{\tilde{Y}}(x-u) du = 2a^{m_u} \lambda e^{-\frac{(x-\mu_Y)^2}{2\sigma_Y^2}} \int_0^\infty u^{2m_u-1} e^{-au^2+bu} du \\ &= 2a^{m_u} \lambda e^{-\frac{(x-\mu_Y)^2}{2\sigma_Y^2}} e^{\frac{b^2}{4a}} \underbrace{\int_0^\infty u^{2m_u-1} e^{-a\left(u-\frac{b}{2\sqrt{a}}\right)^2} du}_{I_{\tilde{R}}}, \end{aligned} \quad (64)$$

where  $b = (x - \mu_Y) / \sigma_Y^2$ . Here,  $a$  and  $\lambda$  are defined in (15a) and (15a), respectively. The solution to  $I_{\tilde{R}}$  in (64) is given by

$$\begin{aligned} I_{\tilde{R}} &= \frac{1}{a^{m_u}} \int_{\frac{-b}{2\sqrt{a}}}^\infty \left( t + \frac{b}{2\sqrt{a}} \right)^{2m_u-1} e^{-t^2} dt = \frac{1}{a^{m_u}} \sum_{k=0}^{2m_u-1} \binom{2m_u-1}{k} \left( \frac{b}{2\sqrt{a}} \right)^{2m_u-1-k} \int_{\frac{-b}{2\sqrt{a}}}^\infty t^k e^{-t^2} dt \\ &\stackrel{(d)}{=} \frac{1}{2a^{m_u}} \sum_{k=0}^{2m_u-1} \binom{2m_u-1}{k} \left( \frac{b}{2\sqrt{a}} \right)^{2m_u-1-k} \Gamma \left( \frac{k+1}{2}, \frac{b^2}{4a} \right), \end{aligned} \quad (65)$$

where step (d) is due to [25, Eq. (2.33.10)]. By substituting (b) and (65) into (64), the PDF of  $\tilde{R}$  is derived as (14).

APPENDIX C  
THE DERIVATION OF CDF OF  $\tilde{R}$  IN (18)

By substituting (14) into (18),  $I_k$  in (18) can be given as

$$\begin{aligned} I_k &= \int_x^\infty e^{-\Delta\left(\frac{u-\mu_Y}{q}\right)^2} \left(\frac{u-\mu_Y}{q}\right)^{2m_u-1-k} \Gamma\left(\frac{k+1}{2}, \left(\frac{u-\mu_Y}{q}\right)^2\right) du \\ &\stackrel{(e)}{=} q \int_{l_{min}}^\infty e^{-\Delta t^2} t^{2m_u-1-k} \Gamma\left(\frac{k+1}{2}, t^2\right) dt, \end{aligned} \quad (66)$$

where  $q = 2\sigma_Y^2\sqrt{a}$ ,  $l_{min} = (x - \mu_Y)/q$ , and the step (e) is written by changing the variable of integration. Then, we divide  $I_k$  into two integrals: (i)  $I_k^o$  for odd values of  $k$  and (ii)  $I_k^e$  for even values of  $k$ . Thus, for odd values of  $k$  and when  $x - \mu_Y < 0$ , this integral can be written as

$$I_k^o = q \underbrace{\int_{l_{min}}^0 e^{-\Delta t^2} t^{2m_u-1-k} \Gamma\left(\frac{k+1}{2}, t^2\right) dt}_{I_{k1}^o} + q \underbrace{\int_0^\infty e^{-\Delta t^2} t^{2m_u-1-k} \Gamma\left(\frac{k+1}{2}, t^2\right) dt}_{I_{k2}^o}. \quad (67)$$

Then, the first integral  $I_{k1}^o$  in (67) can be computed as

$$\begin{aligned} I_{k1}^o &\stackrel{(f)}{=} \int_0^{-l_{min}} e^{-\Delta y^2} y^{2m_u-1-k} \Gamma\left(\frac{k+1}{2}, y^2\right) dy \stackrel{(g)}{=} (\gamma_o - 1)! \sum_{i=0}^{\gamma_o-1} \frac{1}{i!} \int_0^{-l_{min}} e^{-(\Delta+1)y^2} y^{2m_u-1-k} dy \\ &\stackrel{(h)}{=} \frac{(\gamma_o - 1)!}{2} \sum_{i=0}^{\gamma_o-1} \frac{(\Delta+1)^{k/2-m_u-i}}{i!} \int_0^{l_{min}^2(\Delta+1)} v^{m_u+i-k/2} e^{-v} dv \\ &\stackrel{(i)}{=} \frac{(\gamma_o - 1)!}{2} \sum_{i=0}^{\gamma_o-1} \frac{(\Delta+1)^{k/2-m_u-i}}{i!} \gamma\left(m_u+i-\frac{k}{2}, (\Delta+1)l_{min}^2\right), \end{aligned} \quad (68)$$

where the step (f) and step (h) are obtained by substituting  $t = -y$  and  $v = (\Delta+1)y^2$ , respectively. The step (g) is computed via the fact that  $\Gamma(n, x) = (n-1)!e^{-x} \sum_{m=0}^{n-1} x^m/m!$  [25, Eq. (8.352.7)]. The step (i) is written by using [25, Eq. (8.350.1)]. The second integral  $I_{k2}^o$  in (67) can be computed as

$$\begin{aligned} I_{k2}^o &= \int_0^\infty e^{-\Delta t^2} t^{2m_u-1-k} \Gamma\left(\frac{k+1}{2}, t^2\right) dt \stackrel{(j)}{=} (\gamma_o - 1)! \sum_{i=0}^{\gamma_o-1} \frac{1}{i!} \int_0^\infty t^{2m_u+2i-1-k} e^{-(\Delta+1)t^2} dt \\ &\stackrel{(k)}{=} \frac{(\gamma_o - 1)!}{2} \sum_{i=0}^{\gamma_o-1} \frac{(\Delta+1)^{k/2-m_u-i}}{i!} \Gamma\left(m_u+i-\frac{k}{2}\right), \end{aligned} \quad (69)$$

where the step ( $j$ ) is derived via a similar technique used in the step ( $g$ ), and the step ( $k$ ) is evaluated by using [25, Eq. (2.33.10)]. Then, for  $x - \mu_Y > 0$ ,  $I_k^o$  can be calculated as

$$\begin{aligned} I_k^o &= \int_{l_{min}}^{\infty} e^{-\Delta t^2} t^{2m_u-1-k} \Gamma\left(\frac{k+1}{2}, t^2\right) dt = (\gamma_o - 1)! \sum_{i=0}^{\gamma_o-1} \frac{1}{i!} \int_{l_{min}}^{\infty} t^{2m_u+2i-1-k} e^{-(\Delta+1)t^2} dt \\ &= \frac{(\gamma_o - 1)!}{2} \sum_{i=0}^{\gamma_o-1} \frac{(\Delta+1)^{k/2-m_u-i}}{i!} \Gamma\left(m_u + i - \frac{k}{2}, (\Delta+1)l_{min}^2\right). \end{aligned} \quad (70)$$

By combining (67) and (70),  $I_k^o$  can be derived as (20). Then, for even values of  $k$ , the integral in (66) can be evaluated as

$$\begin{aligned} I_k^e &= q \int_{l_{min}}^{\infty} e^{-\Delta t^2} t^{2m_u-1-k} \Gamma\left(\frac{k+1}{2}, t^2\right) dt \quad (71) \\ &\stackrel{(l)}{=} \frac{(\gamma_e - 1)!}{2} \sum_{j=0}^{\gamma_e-1} \left[ -\frac{e^{-\Delta t^2} t^{2j}}{j! \Delta^{\gamma_e-1}} \Gamma\left(\frac{k+1}{2}, t^2\right) \right]_{l_{min}}^{\infty} - (\gamma_e - 1)! \sum_{j=0}^{\gamma_e-1} \frac{\Delta^{\gamma_e-1}}{j!} \int_{l_{min}}^{\infty} t^{k+2j} e^{-(\Delta-1)t^2} dt \\ &= \frac{(\gamma_e - 1)!}{2} \sum_{j=0}^{\gamma_e-1} \frac{e^{-\Delta l_{min}^2} l_{min}^{2j}}{j! \Delta^{\gamma_e-1}} \Gamma\left(\frac{k+1}{2}, l_{min}^2\right) - \frac{(\gamma_e - 1)!}{2} \sum_{j=0}^{\gamma_e-1} \frac{\Delta^{\gamma_e-1}}{j!} \frac{\Gamma\left(j + \frac{k}{2} + \frac{1}{2}, (\Delta+1)l_{min}^2\right)}{(\Delta+1)^{j+k/2+1/2}}, \end{aligned}$$

where the step ( $l$ ) is obtained by using the part-by-part integration technique.

## APPENDIX D

### A. The derivation of expectation of $\tilde{\gamma}^*$ in (32)

The expectation term in (32) can be computed as

$$\begin{aligned} \mathbb{E}[\tilde{\gamma}^*] &= \mathbb{E}[\tilde{\gamma} \tilde{R}^2] = \tilde{\gamma} \mathbb{E}[(\alpha_u + \tilde{Y})^2] = \tilde{\gamma} \sum_{n=0}^2 \binom{2}{n} \mathbb{E}[\alpha_u^{(2-n)}] \mathbb{E}[\tilde{Y}^n] \\ &= \tilde{\gamma} (\sigma_u^2 + \mu_u^2 + \sigma_Y^2 + \mu_Y^2 + 2\mu_u \mu_Y), \end{aligned} \quad (72)$$

where  $\mu_Y$ ,  $\sigma_Y^2$ ,  $\mu_u$ , and  $\sigma_u^2$  are given in (13a), (13b), (33a), and (33b), receptively.

### B. The derivation of variance of $\tilde{\gamma}^*$ in (35)

The first expectation term in (35) can be evaluated as

$$\mathbb{E}[\tilde{R}^4] = \mathbb{E}[(\alpha_u + \tilde{Y})^4] = \sum_{n=0}^4 \binom{4}{n} \mathbb{E}[\alpha_u^{(4-n)}] \mathbb{E}[\tilde{Y}^n]. \quad (73)$$

Thus, the  $n$ th moment of  $\alpha_u^n$  denoted by  $\mathbb{E}[\alpha_u^n]$  can be computed as

$$\begin{aligned} \mathbb{E}[\alpha_u^n] &= \int_0^{\infty} x^n f_u(x) dx = \frac{2m_u^{m_u}}{\Gamma(m_u) \xi_u^{m_u}} \int_0^{\infty} x^{2m_u+n-1} e^{-\frac{m_u x^2}{\xi_u}} dx \\ &\stackrel{(m)}{=} \frac{\xi_u^{n/2}}{\Gamma(m_u) m_u^{n/2}} \Gamma(m_u + n/2), \end{aligned} \quad (74)$$



where the step ( $m$ ) is evaluated by using [25, Eq. (2.33.10)]. Then,  $\mathbb{E}[\tilde{Y}^n]$  can be derived as

$$\begin{aligned}\mathbb{E}[\tilde{Y}^n] &= \frac{\psi}{\sqrt{2\pi\sigma_Y^2}} \int_0^\infty y^n e^{-\frac{(y-\mu_Y)^2}{2\sigma_Y^2}} dy \stackrel{(n)}{=} \frac{\psi}{\sqrt{\pi}} \int_{\frac{-\mu_Y}{\sqrt{2\sigma_Y^2}}}^\infty \left(\sqrt{2\sigma_Y^2}t + \mu_Y\right)^n e^{-t^2} dt \\ &\stackrel{(o)}{=} \frac{\psi}{2\sqrt{\pi}} \sum_{i=0}^n \binom{n}{i} \left(\sqrt{2\sigma_Y^2}\right)^{n-i} \mu_Y^i I\left(n-i, \frac{-\mu_Y}{2\sigma_Y^2}\right),\end{aligned}\quad (75)$$

where the step ( $n$ ) is due to a changing of variable and the step ( $o$ ) is obtained by expanding  $\left(\sqrt{2\sigma_Y^2}t + \mu_Y\right)^n$  based on  $n$  value. Moreover,  $I(\cdot, \cdot)$  is given in (39).

*C. The derivation of the asymptotic achievable rate ( $\mathcal{R}^\infty$ ) as  $L \rightarrow \infty$  in (43)*

When the number of IRS elements grows without bound ( $L \rightarrow \infty$ ),  $\mu_Y$  in (13a) and  $\sigma_Y^2$  in (13b) can be approximated as

$$\mu_Y \approx L\bar{\mu}_Y = L \left( \sum_{n=1}^N \eta_n \sqrt{\frac{\xi_{h_n} \xi_{g_n}}{m_h m_g}} \frac{\Gamma(m_h + 1/2) \Gamma(m_g + 1/2)}{\Gamma(m_h) \Gamma(m_g)} \right), \quad (76)$$

$$\sigma_Y^2 \approx L\bar{\sigma}_Y^2 = L \left( \sum_{n=1}^N \eta_n^2 \left( \frac{\xi_{h_n} \xi_{g_n}}{m_h m_g} \right) \frac{\Gamma(m_h + 1) \Gamma(m_g + 1)}{\Gamma(m_h) \Gamma(m_g)} - \bar{\mu}_Y^2 \right), \quad (77)$$

where  $\eta_n = \eta_{nl}$ . Thus, the SNR term in  $\mathcal{R}_{ub}$  (41) can be asymptotically evaluated as

$$\lim_{L \rightarrow \infty} \gamma_{ub} = \lim_{L \rightarrow \infty} \bar{\gamma} L^2 \left( \frac{\sigma_u^2}{L^2} + \frac{\bar{\sigma}_Y^2}{L} + \frac{2\mu_u \bar{\mu}_Y}{L} + \frac{\mu_u^2}{L^2} + \bar{\mu}_Y^2 \right) = \bar{\gamma}_E \bar{\mu}_Y^2, \quad (78)$$

where  $\bar{\gamma}_E = P_E/\sigma_w^2$  and  $\lim_{L \rightarrow \infty} P = P_E/L^2$ . Similarly, in the asymptotic regime, the SNR term in  $\mathcal{R}_{lb}$  (40) can be derived as

$$\lim_{L \rightarrow \infty} \gamma_{lb} = \lim_{L \rightarrow \infty} \bar{\gamma} \left( \frac{L^6 \left( \frac{\sigma_u^2}{L^2} + \frac{\bar{\sigma}_Y^2}{L} + \frac{2\mu_u \bar{\mu}_Y}{L} + \frac{\mu_u^2}{L^2} + \bar{\mu}_Y^2 \right)^3}{L^4 \left( \frac{\psi}{2\sqrt{\pi}} \bar{\mu}_Y^4 I\left(0, \frac{-\sqrt{L}\bar{\mu}_Y}{\sqrt{2\sigma_Y^2}}\right) + \frac{\Upsilon(L^3)}{L^4} \right)} \right) = \lim_{L \rightarrow \infty} \bar{\gamma} L^2 \left( \frac{\bar{\mu}_Y^2}{\frac{\psi}{2\sqrt{\pi}} I(0, -\infty)} \right) \stackrel{(p)}{=} \bar{\gamma}_E \bar{\mu}_Y^2, \quad (79)$$

where  $\Upsilon(L^3)$  is lower order ( $L < 4$ ) terms of the expansion of the SNR in (40). Moreover, the step ( $p$ ) is written by using the fact that  $\lim_{L \rightarrow \infty} \psi = \lim_{L \rightarrow \infty} 1/\mathcal{Q}\left(-\sqrt{L}\bar{\mu}_Y/\bar{\sigma}_Y\right) = \lim_{L \rightarrow \infty} 1/\mathcal{Q}(-\infty) = 1$  and  $I(0, -\infty) = 2\Gamma(1/2) = 2\sqrt{\pi}$ . Then, the asymptotic achievable rate  $\mathcal{R}^\infty$  can be derived as given in (43).

APPENDIX E  
THE DERIVATION OF THE AVERAGE SER IN (47)

The inner expectation term with respect to  $\tilde{Y}$  in (46) can be evaluated via a tight approximation [32] for the Gaussian  $Q$ -function:  $Q(x) \approx \exp(-cx^2 - dx)/2$ , where  $c = 0.374$  and  $d = 0.777$  as follows:

$$\mathbb{E}_{\tilde{Y}} \left[ Q \left( \vartheta_b(\alpha_u + \tilde{Y}) \right) \right] = \frac{1}{2} \int_0^\infty e^{-cx^2 - dx} f_{\tilde{Y}}(y) dy = \frac{\psi e^{-c\vartheta_b^2 \alpha_u^2 - d\vartheta_b \alpha_u - \frac{\mu_{\tilde{Y}}^2}{2\sigma_{\tilde{Y}}^2}}}{2\sqrt{2\pi\sigma_{\tilde{Y}}^2}} \underbrace{\int_0^\infty e^{-a_1 y^2 - a_2 y} dy}_{I_{\tilde{Y}}}, \quad (80)$$

where  $a_1 = c\vartheta_b^2 + 1/2\sigma_{\tilde{Y}}^2$  and  $a_2 = 2c\vartheta_b^2 \alpha_u + d\vartheta_b - \mu_{\tilde{Y}}/\sigma_{\tilde{Y}}^2$ . Then, the integral  $I_{\tilde{Y}}$  in (80) can be evaluated by first using a substitution  $t = y + a_2/(2a_1)$  and then invoking [25, Eq. (2.33.16)]

$$\begin{aligned} I_{\tilde{Y}} &= \exp\left(\frac{a_2^2}{4a_1^2}\right) \int_0^\infty \exp\left(-a_1 \left(y + \frac{a_2}{2a_1}\right)^2\right) dy = \exp\left(\frac{a_2^2}{4a_1^2}\right) \int_{a_2/2a_1}^\infty \exp(-a_1 t^2) dt \\ &= \frac{1}{2} \sqrt{\frac{\pi}{a_1}} \exp\left(\frac{a_2^2}{4a_1^2}\right) \operatorname{erfc}\left(\frac{a_2}{2\sqrt{a_1}}\right). \end{aligned} \quad (81)$$

Then, by substituting  $a_2$  and (81) into (80), the inner expectation in (46) can be rewritten as

$$\mathbb{E}_{\tilde{Y}} \left[ Q \left( \vartheta_b(\alpha_u + \tilde{Y}) \right) \right] = \frac{\psi e^{-c\vartheta_b^2 \alpha_u^2 - d\vartheta_b \alpha_u - \frac{\mu_{\tilde{Y}}^2}{2\sigma_{\tilde{Y}}^2}}}{4\sqrt{2\sigma_{\tilde{Y}}^2 a_1}} \exp(-v' \alpha_u^2 - u_1 \alpha_u) \operatorname{erfc}(s\alpha_u + r), \quad (82)$$

where  $v' = v_1 - m_u/P_u$ . Moreover,  $S$ ,  $r$ ,  $u_1$ , and  $v_1$  are defined in (49b), (49c), (49d), and (49f), respectively. By substituting (82) into (46), the outer expectation with respect to  $\alpha_u$  can be written as

$$\begin{aligned} \mathbb{E}_{\alpha_u} \left[ \mathbb{E}_{\tilde{Y}} \left[ Q \left( \vartheta_b(\alpha_u + \tilde{Y}) \right) \right] \right] &= \int_0^\infty \mathbb{E}_{\tilde{Y}} \left[ Q \left( \vartheta_b(\alpha_u + \tilde{Y}) \right) \right] f_u(\alpha_u) d\alpha_u \\ &= 2\sqrt{2\pi} B \underbrace{\int_0^\infty \alpha_u^{2m_u-1} e^{-v_1 \left(\alpha_u + \frac{u_1}{2v_1}\right)^2} Q \left( \sqrt{2}(s\alpha_u + r) \right) d\alpha_u}_{I_{\alpha_u}}, \end{aligned} \quad (83)$$

where  $B$  is defined in (49a). Then, the integral  $I_{\alpha_u}$  in (83) can be evaluated as

$$\begin{aligned} I_{\alpha_u} &= \int_0^\infty \alpha_u^{2m_u-1} e^{-v_1 \left(\alpha_u + \frac{u_1}{2v_1}\right)^2} Q \left( \sqrt{2}(s\alpha_u + r) \right) d\alpha_u \quad (84) \\ &\stackrel{(q)}{=} \frac{-1}{2} \sum_{k=0}^{2m_u-1} \left(\frac{-u_1}{2v_1}\right)^{2m_u-1-k} \Gamma(\gamma_b) \left[ Q \left( \sqrt{2}(s\alpha_u + r) \right) e^{-v_1 \left(\alpha_u + \frac{u_1}{2v_1}\right)^2} \sum_{i=0}^{\gamma_b-1} \frac{(\alpha_u + u_1/2v_1)^{2i}}{i! v_1^{\gamma_b-i}} \right]_0^\infty \\ &\quad - \frac{s}{2\sqrt{\pi}} \sum_{k=0}^{2m_u-1} \left(\frac{-u_1}{2v_1}\right)^{2m_u-1-k} \Gamma(\gamma_b) \sum_{i=0}^{\gamma_b-1} \frac{1}{i! v_1^{\gamma_b-i}} \int_0^\infty \left(\alpha_u + \frac{u_1}{2v_1}\right)^{2i} e^{-v_1 \left(\alpha_u + \frac{u_1}{2v_1}\right)^2 - (s\alpha_u + r)^2} d\alpha_u \end{aligned}$$

$$\begin{aligned}
&= \frac{Q(\sqrt{2}r)}{2} \sum_{k=0}^{2m_u-1} \left(\frac{-u_1}{2v_1}\right)^{2m_u-1-k} \Gamma(\gamma_b) \sum_{i=0}^{\gamma_b-1} \frac{(u_1/2v_1)^{2i}}{i!v_1^{\gamma_b-i}} \\
&\quad - \frac{s}{2\sqrt{\pi}} \sum_{k=0}^{2m_u-1} \left(\frac{-u_1}{2v_1}\right)^{2m_u-1-k} \Gamma(\gamma_b) \sum_{i=0}^{\gamma_b-1} \frac{1}{i!v_1^{\gamma_b-i}} \underbrace{\int_0^\infty \left(\alpha_u + \frac{u_1}{2v_1}\right)^{2i} e^{-v_1\left(\alpha_u + \frac{u_1}{2v_1}\right)^2 - (s\alpha_u+r)^2} d\alpha_u}_{I_{\alpha'_u}},
\end{aligned}$$

where  $\gamma_b = (k+1)/2$ . The step (q) is written by using the part-by-part integration technique. Then, the integral  $I_{\alpha'_u}$  can be rearranged as follows:

$$\begin{aligned}
I_{\alpha'_u} &= e^{\frac{u_2^2}{4v_2} - \frac{u_1^2}{4v_1} - r} \int_0^\infty \left(\alpha_u + \frac{u_1}{2v_1}\right)^{2i} e^{-v_2\left(\alpha_u + \frac{u_2}{2v_2}\right)^2} d\alpha_u \\
&\stackrel{(r)}{=} e^{\frac{u_2^2}{4v_2} - \frac{u_1^2}{4v_1} - r} \sum_{j=0}^{2i} q_b^{2i-j} \int_{\frac{u_2}{2v_2}}^\infty t^j e^{-v_2 t^2} dt = e^{\frac{u_2^2}{4v_2} - \frac{u_1^2}{4v_1} - r} \sum_{j=0}^{2i} q_b^{2i-j} I_b,
\end{aligned} \tag{85}$$

where  $q_b = u_1/2v_1 - u_2/2v_2$  and  $I_b$  is defined in (48). Further, the step (r) is obtained via the substitution  $t = \alpha_u + u_2/(2v_2)$ . Finally,  $u_2$  and  $v_2$  are defined in (49e) and (49g), respectively.

#### APPENDIX F THE DERIVATION OF $P_{out}^\infty$ IN (52) AND $\bar{P}_e^\infty$ IN (58)

From (61) in Appendix A, the PDF of  $z_{nl} = \alpha_{h_{nl}}\alpha_{g_{nl}}$  can be written as

$$f_{z_{nl}}(x) = \alpha' x^{m_s+m_l-1} \mathcal{K}_{m_s-m_l} \left( 2x\sqrt{m_s m_l / (\xi_{s_n} \xi_{l_n})} \right), \tag{86}$$

where  $\alpha'$  is given in (55b),  $m_s = \min(m_h, m_g)$ , and  $m_l = \max(m_h, m_g)$ . Moreover,  $\xi_{s_n}$  and  $\xi_{l_n}$  are the scaling parameters of the respective channel models (3). The moment generating function (MGF) of  $z_{nl}$  can be derived by evaluating the Laplace transform of  $f_{z_{nl}}(x)$  as [26]

$$\begin{aligned}
\mathcal{M}_{z_{nl}}(s) &= \int_0^\infty f_{z_{nl}}(x) \exp(-sx) dx = \alpha' \int_0^\infty x^{m_s+m_l-1} e^{-sx} \mathcal{K}_{m_s-m_l} \left( 2x\sqrt{m_s m_l / (\xi_{s_n} \xi_{l_n})} \right) dx \tag{87} \\
&\stackrel{(s)}{=} \frac{\alpha' \pi (2b_n)^{(m_s-m_l)} \Gamma(2m_s) \Gamma(2m_l)}{\Gamma(m_s+m_l+1/2)} (s+b_n)^{2m_s} F \left( 2m_s, m_s-m_l+\frac{1}{2}; m_s+m_l+\frac{1}{2}; \frac{s-b_n}{s+b_n} \right),
\end{aligned}$$

where  $b_n = 2\sqrt{m_s m_l / (\xi_{h_n} \xi_{g_n})}$  and  $F(\cdot, \cdot; \cdot; \cdot)$  is the Gauss Hypergeometric function [25, Eq. (9.100)]. In (87), the step (s) is derived by using [25, Eq. (6.621.3)]. The behavior of the PDF of  $z_{nl}$  at the origin is governed by the asymptotic value of  $\mathcal{M}_{z_{nl}}(s)$  as  $s \rightarrow \infty$  [33]. To this end, by using the fact that  $\lim_{s \rightarrow \infty} (s-b_n)/(s+b_n) \rightarrow 1$ , and since  $m_s < m_l$ , we invoke [25, Eq. (9.122.1)] to evaluate  $\mathcal{M}_{z_{nl}}(s)$  when  $s \rightarrow \infty$  as follows:

$$\mathcal{M}_{z_{nl}}^\infty(s) = \theta_n s^{-2m_s}, \tag{88}$$

where  $\theta_n$  is defined in (55a). Thus, the MGF of  $Y = \sum_{n=1}^N \sum_{l=1}^L \eta_{nl} z_{nl}$  as  $s \rightarrow \infty$  is given by

$$\mathcal{M}_Y^\infty(s) = \prod_{n=1}^N \prod_{l=1}^L \eta_{nl} \theta_n s^{-2m_s} = \Phi(N, L) s^{-2m_s NL}, \quad (89)$$

where  $\Phi(N, L)$  is given in (54). Then, the PDF of the direct channel envelope ( $u$ ) can be expanded at the origin by using the Maclaurin series expansion of the exponential function [25, Eq. (0.318.2)] as

$$\begin{aligned} f_{\alpha_u}(x) &= \frac{2m_u^{m_u} x^{2m_u-1}}{\Gamma(m_u) \xi_u^{m_u}} \exp\left(\frac{-x^2}{\xi_u}\right) = \frac{2m_u^{m_u} x^{2m_u-1}}{\Gamma(m_u) \xi_u^{m_u}} \sum_{k=0}^{\infty} \frac{1}{k!} \left(\frac{-x^2}{\xi_u}\right)^k \\ &= \frac{2m_u^{m_u} x^{2m_u-1}}{\Gamma(m_u) \xi_u^{m_u}} \left(1 - \frac{x^2}{\xi_u} + \frac{x^4}{2\xi_u^2} - \frac{x^6}{6\xi_u^3} + \dots\right). \end{aligned} \quad (90)$$

Then, the PDF of the direct channel envelope ( $u$ ) for  $x \rightarrow 0^+$  can be approximated as

$$f_{\alpha_u}^{0+}(x) = \frac{2m_u^{m_u} x^{2m_u-1}}{\Gamma(m_u) \xi_u^{m_u}} + \mathcal{O}(x^{2m_u}). \quad (91)$$

By computing the Laplace transform of (91), we obtain the asymptotic MGF of  $\alpha_u$  as [25, Eq. (17.13.2)]

$$\mathcal{M}_{\alpha_u}^\infty(s) = \frac{2m_u^{m_u} \Gamma(2m_u)}{\Gamma(m_u) \xi_u^{m_u}} s^{-2m_u}. \quad (92)$$

Then, the asymptotic MGF of  $R = \alpha_u + Y$  for  $s \rightarrow \infty$  can be derived as

$$\mathcal{M}_R^\infty(s) = \mathcal{M}_{z_{nl}}(s) \mathcal{M}_{\alpha_u}^\infty(s) = \frac{\Phi(N, L) 2m_u^{m_u} \Gamma(2m_u)}{\Gamma(m_u) \xi_u^{m_u}} s^{-2m_s NL - 2m_u}, \quad (93)$$

where  $\Phi(N, L)$  is defined in (54). By taking inverse Laplace transform of (93) [25], the PDF of  $R$  for  $x \rightarrow 0^+$  can be computed as

$$f_R^{0+}(x) \stackrel{(t)}{=} \frac{\Phi(N, L) 2m_u^{m_u} \Gamma(2m_u)}{\Gamma(m_u) \xi_u^{m_u} \Gamma(2m_s NL + 2m_u)} x^{2m_s NL + 2m_u - 1} + \mathcal{O}(x^{2m_s NL + 2m_u}), \quad (94)$$

where the step (t) is written by using [25, Eq. (17.13.3)]. Next, the CDF of  $R$  for  $x \rightarrow 0^+$  is given as

$$\begin{aligned} F_R^{0+}(x) &= \int_0^x f_R^{0+}(u) du = \int_0^x \frac{\Phi(N, L) 2m_u^{m_u} \Gamma(2m_u)}{\Gamma(m_u) \xi_u^{m_u} \Gamma(2m_s NL + 2m_u)} u^{2m_s NL + 2m_u - 1} du + \mathcal{O}(u^{2m_s NL + 2m_u}) \\ &= \frac{\Phi(N, L) 2m_u^{m_u} \Gamma(2m_u)}{2G_d \Gamma(m_u) \xi_u^{m_u} \Gamma(2G_d)} x^{2G_d} + \mathcal{O}(x^{2G_d+1}), \end{aligned} \quad (95)$$

where  $G_d = m_s NL + m_u$ . Then, the CDF of  $\gamma^* = \bar{\gamma} R^2$  for  $x \rightarrow 0^+$  can be approximated as [26]

$$F_{\gamma^*}^{0+}(x) = \Pr(\gamma^* \leq x) \approx F_R^{0+}\left(\sqrt{x/\bar{\gamma}}\right) = \frac{\Phi(N, L) 2m_u^{m_u} \Gamma(2m_u)}{2G_d \Gamma(m_u) \xi_u^{m_u} \Gamma(2G_d)} \left(\frac{x}{\bar{\gamma}}\right)^{G_d} + \mathcal{O}\left(\left(\frac{x}{\bar{\gamma}}\right)^{G_d+1}\right). \quad (96)$$

Thereby, the asymptotic outage probability can be computed as

$$P_{out}^{\infty} \approx F_{\gamma^*}^{0+}(\gamma_{th}) = \Omega \Phi(N, L) \left( \frac{\gamma_{th}}{\bar{\gamma}} \right)^{G_d} + \mathcal{O} \left( \left( \frac{\gamma_{th}}{\bar{\gamma}} \right)^{G_d+1} \right), \quad (97)$$

where  $\Omega$  is given in (54). Finally, the asymptotic average BER can be derived as follows:

$$\begin{aligned} P_e^{\infty} &= \int_0^{\infty} \omega \mathcal{Q}(\sqrt{\vartheta x}) f_{\gamma^*}^{0+}(x) dx = \frac{\omega}{2} \sqrt{\frac{\vartheta}{2\pi}} \int_0^{\infty} x^{-1/2} \exp\left(\frac{-\vartheta x}{2}\right) F_{\gamma^*}^{0+}(x) dx \\ &= \frac{\omega}{2} \sqrt{\frac{\vartheta}{2\pi}} \frac{\Phi(N, L) 2m_u^{m_u} \Gamma(2m_u)}{2G_d \Gamma(m_u) \xi_u^{m_u} \Gamma(2G_d)} \bar{\gamma}^{-G_d} \int_0^{\infty} x^{G_d-1/2} \exp\left(\frac{-\vartheta x}{2}\right) dx + \mathcal{O} \left( \left( \frac{x}{\bar{\gamma}} \right)^{G_d+1} \right) \\ &\stackrel{(u)}{=} \Lambda \Phi(N, L) \bar{\gamma}^{-G_d} + \mathcal{O}(\bar{\gamma}^{-(G_d+1)}), \end{aligned} \quad (98)$$

where  $\Lambda$  is given in (59) and the step (u) is computed via [25, Eq. (3.326.2)].

## REFERENCES

- [1] D. L. Galappaththige, D. Kudathanthirige, and G. Amarasuriya Aruma Baduge, "Performance Analysis of Distributed Intelligent Reflective Surface Aided Communications," in *IEEE Global Communications Conference (GLOBECOM)*, May 2020, pp. 1–6, (submitted).
- [2] C. Liaskos *et al.*, "A New Wireless Communication Paradigm Through Software-Controlled Metasurfaces," *IEEE Commun. Mag.*, vol. 56, no. 9, pp. 162–169, 2018.
- [3] M. Di Renzo *et al.*, "Smart Radio Environments Empowered by Reconfigurable AI Meta-Surfaces: An idea whose time has come," *EURASIP J. Wireless Commun. Net.*, May 2019.
- [4] T. Sekitani *et al.*, "Stretchable Active-Matrix Organic Light-Emitting Diode Display Using Printable Elastic Conductors," *Nature Materials*, vol. 11, no. 11, p. 494–499, 2009.
- [5] S. Zhang, Q. Wu, S. Xu, and G. Y. Li, "Fundamental Green Tradeoffs: Progresses, Challenges, and Impacts on 5G Networks," *IEEE Communications Surveys Tutorials*, vol. 19, no. 1, pp. 33–56, 2017.
- [6] R. Karasik, O. Simeone, M. D. Renzo, and S. Shamai, "Beyond Max-SNR: Joint Encoding for Reconfigurable Intelligent Surfaces," *ArXiv*, vol. abs/1911.09443, 2019.
- [7] E. Basar *et al.*, "Wireless Communications Through Reconfigurable Intelligent Surfaces," vol. 7, pp. 116 753–116 773, 2019.
- [8] W. Tang *et al.*, "Wireless Communications with Reconfigurable Intelligent Surface: Path Loss Modeling and Experimental Measurement," *arXiv:1911.05326*, Nov. 2019.
- [9] Q. Wu and R. Zhang, "Intelligent Reflecting Surface Enhanced Wireless Network via Joint Active and Passive Beamforming," *IEEE Trans. Wireless Commun.*, pp. 1–1, 2019.
- [10] —, "Beamforming Optimization for Wireless Network Aided by Intelligent Reflecting Surface with Discrete Phase Shifts," *IEEE Trans. Commun.*, vol. 68, no. 3, pp. 1838–1851, 2020.
- [11] C. Huang, A. Zappone, G. C. Alexandropoulos, M. Debbah, and C. Yuen, "Reconfigurable Intelligent Surfaces for Energy Efficiency in Wireless Communication," *IEEE Trans. Wireless Commun.*, vol. 18, no. 8, pp. 4157–4170, 2019.
- [12] D. Kudathanthirige, D. Gunasinghe, and G. Amarasuriya, "Performance Analysis of Intelligent Reflective Surfaces for Wireless Communication," in *IEEE International Conference on Communications (ICC)*, June 2020, pp. 1–6.

- [13] Y. Han, W. Tang, S. Jin, C. Wen, and X. Ma, "Large Intelligent Surface-Assisted Wireless Communication Exploiting Statistical CSI," *IEEE Trans. Veh. Technol.*, vol. 68, no. 8, pp. 8238–8242, Aug 2019.
- [14] J. Chen, Y. Liang, Y. Pei, and H. Guo, "Intelligent Reflecting Surface: A Programmable Wireless Environment for Physical Layer Security," vol. 7, pp. 82 599–82 612, 2019.
- [15] E. Basar, "Transmission Through Large Intelligent Surfaces: A New Frontier in Wireless Communications," *European Conference on Networks and Communications (EuCNC)*, pp. 112–117, 2019.
- [16] S. Abeywickrama, R. Zhang, Q. Wu, and C. Yuen, "Intelligent reflecting surface: Practical phase shift model and beamforming optimization," *IEEE Trans. Commun.*, 2020, accepted.
- [17] S. Zhang and R. Zhang, "Intelligent Reflecting Surface Aided Multiple Access: Capacity Region and Deployment Strategy," *arXiv:2002.07091*, 2020.
- [18] M. Jung, W. Saad, M. Debbah, and C. S. Hong, "On the Optimality of Reconfigurable Intelligent Surfaces (RISs): Passive Beamforming, Modulation, and Resource Allocation," *arXiv:1910.00968*, 2019.
- [19] M. Jung, W. Saad, Y. Jang, G. Kong, and S. Choi, "Reliability Analysis of Large Intelligent Surfaces (LISs): Rate Distribution and Outage Probability," vol. 8, no. 6, pp. 1662–1666, 2019.
- [20] C. Guo, Y. Cui, F. Yang, and L. Ding, "Outage Probability Analysis and Minimization in Intelligent Reflecting Surface-Assisted MISO Systems," *IEEE Commun. Lett.*, pp. 1–1, 2020.
- [21] S. Hu and F. Rusek, "Spherical Large Intelligent Surfaces," *IEEE International Conference on Acoustics, Speech and Signal Processing*, pp. 8673–8677, 2020.
- [22] C. Psomas and I. Krikidis, "Low-Complexity Random Rotation-based Schemes for Intelligent Reflecting Surfaces," *arXiv:1912.10347*, 2019.
- [23] M. Cui, G. Zhang, and R. Zhang, "Secure Wireless Communication via Intelligent Reflecting Surface," vol. 8, no. 5, pp. 1410–1414, 2019.
- [24] X. Guan, Q. Wu, and R. Zhang, "Intelligent Reflecting Surface Assisted Secrecy Communication: Is Artificial Noise Helpful or Not?" vol. 9, no. 6, pp. 778–782, 2020.
- [25] I. Gradshteyn and I. Ryzhik, *Table of Integrals, Series, and Products*, 7th ed. Academic Press, 2007.
- [26] A. Papoulis and S. U. Pillai, *Probability, Random Variables, and Stochastic Processes*, 4th ed. McGraw Hill, 2002.
- [27] Q. Wu and R. Zhang, "Towards Smart and Reconfigurable Environment: Intelligent Reflecting Surface Aided Wireless Network," *IEEE Commun. Mag.*, vol. 58, no. 1, pp. 106–112, 2020.
- [28] T. M. Cover and J. A. Thomas, *Elements of Information Theory*. USA: Wiley-Interscience, 1991.
- [29] S. Atapattu, C. Tellambura, and H. Jiang, "A Mixture Gamma Distribution to Model the SNR of Wireless Channels," *IEEE Transactions on Wireless Communications*, vol. 10, no. 12, pp. 4193–4203, 2011.
- [30] Q. Zhang, S. Jin, K.-K. Wong, H. Zhu, and M. Matthaiou, "Power Scaling of Uplink Massive MIMO Systems with Arbitrary-Rank Channel Means," *IEEE J. Sel. Areas Signal Process.*, vol. 8, no. 5, pp. 966–981, Oct. 2014.
- [31] J. Proakis, *Digital Communications*, 4th ed. New York:McGraw-Hill, Inc., 2001.
- [32] A. Mastin and P. Jaillet, "Log-Quadratic Bounds for the Gaussian Q-function," *arXiv e-prints*, 2013.
- [33] Z. Wang and G. B. Giannakis, "A Simple and General Parameterization Quantifying Performance in Fading Channels," *IEEE Trans. Commun.*, vol. 51, no. 8, pp. 1389–1398, Aug. 2003.
- [34] T. L. Marzetta, E. G. Larsson, H. Yang, and H. Q. Ngo, *Fundamentals of Massive MIMO*. Cambridge University Press, Cambridge, UK, 2016.